Novel Coatings for Improving the Corrosion Resistance of Mg Biomedical Implants

A report submitted in partial fulfilment of the requirements for the degree of

Bachelor of Science with Honours in Chemistry

at the

School of Physical and Chemical Sciences

University of Canterbury

by

Liam Carroll

under the supervision of

Prof. Alison Downard

and co-supervision of

A/Prof. Mark Staiger

October 2017

Abstract

This study looked at the functionalisation of Mg using aryldiazonium chemistry to decrease the corrosion properties of the metal and successfully modified the surface. Nitrophenyl (NP) films were successfully grafted from water and acetonitrile (ACN) with analysis using water contact angles, infrared spectroscopy, and X-ray photoelectron spectroscopy confirming this. Both water and ACN are suitable media for the reaction of 4-nitrobenzenediazonium and Mg to form NP films. However, water forms an unsuitably thick layer when using 4-ethynylbenzenediazonium. A concentration of 25 mM and reaction time of 4 h are sufficient for multilayer film growth. These thin films do not provide any corrosion protection, indicating an additional bioactive layer will need to protect the metal.

Acknowledgements

I wish to thank my supervisor, Prof. Alison Downard, for her direction and support throughout this project. I would like to acknowledge Dr. Paula Brooksby for her guidance in the lab, Ryan Wilkes for providing the magnesium substrates used in my experiments, and Craig Melton for previous work. I would like to thank Dr. Colin Doyle at the University of Auckland for his assistance with XPS data acquisition. I would also like to thank the Downard Dream Team: Joel, The Schneillmanator; Alex, Captain McSchneill the Vegan; Anna, Queen Julian; and Ting, Kung Fu Wu, for their support and advice throughout the entire year, you guys are the best. Lastly, I would like to thank the Carlisle Charitable Trust for the Walter Jones Scholarship which helped towards the cost of my studies.

Declaration

I, Liam Robert Carroll, declare that all work presented in this report is my own and that acknowledgement is given to previous studies and to my colleagues where it is due.

Signature:_____

Date:_____

Contents

Glossary

ACN	acetonitrile
ABD	4-aminobenzenediazonium
CB	carbonate buffer
EBD	4-ethynylbenzenediazonium
EP	ethynylphenyl
GC	glassy carbon
HA	hydroxyapatite
HEPES	2-(4-(2-hydroxyethyl)piperazin-1-yl)ethane-1-sulfonic acid
LSV	linear sweep voltammetry
NBD	4-nitrobenzenediazonium
NP	4-nitrophenyl
PB	phosphate buffer
PCL	poly(ε-caprolactone)
PCS	photocurrent spectroscopy
PLLA	poly(L-lactic acid)
PLGA	poly(lactic-co-glycolic acid)
PT	pretreatment
SiC	silicon-carbide
WCA	water contact angle
XPS	X-ray photoelectron spectroscopy

1 Introduction

1.1 Limitations of Non-Degradable Implants

Orthopaedics relies on the use of permanent and temporary implants to replace missing joints or bones or to support damaged tissue when trauma has occurred to the musculoskeletal system.[1,2] Due to the composition of the human body, implants are required to withstand a complex environment, while also promoting the regrowth and repair of the body. Implants are constructed from materials which are selected for their high mechanical strength and fracture resistance and are constructed from metals, ceramics, or plastics.[1–4] Common metallic orthopaedic materials include stainless steel, titanium, and cobalt-chromium-based alloys; these are standard due to their high corrosion resistance.

One significant limitation of these materials is the release of toxic corrosion products when degradation eventually occurs.[2,5,6] Whether through mechanical wear or chemical attack, ions and particles can hinder development and growth of the surrounding tissue and cause additional trauma.[5]

Another disadvantage is the mechanical properties exhibited by metals are not well matched with those of natural bone and can result in stress shielding effects.[7,8] According to Wolff's Law, the strength of a bone is proportional to the loads it is placed under, therefore, if a bone is supported by a mechanically stable implant, the bone will become less dense, and weaker.[9] Reduced stimulation for bone regrowth retards the healing process and may prevent a complete recovery.[2,7,9,10]

Additionally, implants are often removed, either after the healing process is complete, or due to complications. Bostman et al. reported that 15 % of all operations (23 % of elective surgeries) within the Helsinki University Hospital orthopaedic and trauma unit was for the removal of implants.[11] Removal leads to repeat operations that increase healthcare costs and unwanted complications and trauma (including further fractures) for the patient.[12] These limitations have resulted in the investigation of biodegradable implants as an alternative biomaterial for some applications.

1.2 Biodegradable Implants

Zheng et al.[13] define biodegradable materials as materials expected to corrode gradually in vivo, with an appropriate host response elicited by released corrosion products, and then dissolve entirely upon fulfilling the mission to assist with tissue healing. The general biological, chemical, physical, and mechanical characteristic of all biodegradable materials are set out in Table 1.

Figure 1 depicts the relationship between the strength of healing bone and permanent and degradable implants. The implant is required to maintain physical and mechanical integrity up until the bone begins to form stronger lamellar bone, requiring pressure to form correctly.[9] When this occurs, a biodegradable implant should degrade within a reasonable period of time which can be sped up by making the implant porous.[13] Permanent implants are not designed to do this and thus induce stress shielding beyond the mechanically sensitive range[7] and require a secondary removal operation.[10]

Table 1: Comparison between permanent and biodegradable materials in biomedical applications.[13]

Items	Permanent materials	Biodegradable materials
Mechanical property	Stable	Degrade with time and should match recovery process (Figure 1)
Corrosion product release	Unwanted	The release of ions/particles should be acceptable by the host locally and all over the body
Interaction with surrounding tissue	Bio-inert	Bio-active
Application fields	Ubiquitous	Specialised

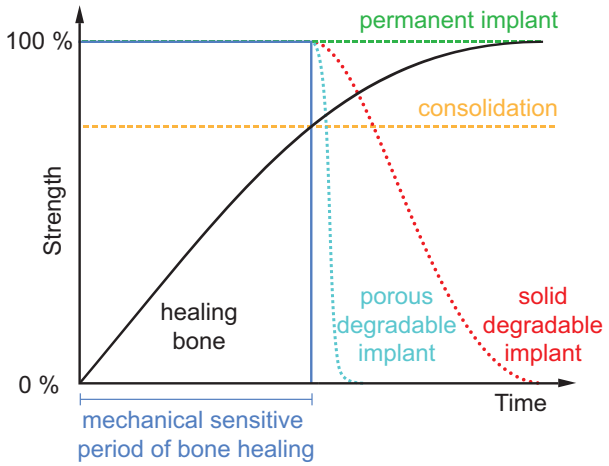

Figure 1. The mechanical strength of bone, permanent implants, and solid and porous degradable implants as the bone heals. Consolidation is the point at which the stronger lamellar bone forms, requiring pressure to form correctly. Modified from reference 13.

Biodegradable materials can be generalised into three categories: polymers, ceramics, and metals, however, composites are also being thoroughly investigated. Polymeric implants were first reported by Kulkarni et al.[14] and are already successful materials for osteosynthesis, where low or mild load bearing applications are required,[13] such as interfacial screws and suture anchors.[15] Polymers provide excellent degradation rate versatility, ranging from 1–2 months to longer than 2 years, with even more variability when copolymers are employed.[16] Ceramics have remarkable biocompatibility, resorbability and bioactivity and furthermore promote bone growth on their surface. Their high mechanical strength and rigidity[2] facilitates their use as a bioactive scaffold which the body uses as a template for tissue repair.

Metallic biomaterials are pure, alloy or composite materials which are non-toxic to the body. Whereas traditional metals (stainless steel, titanium and cobalt-chromium alloys) have high corrosion resistance in the body, biodegradable metals are selected for their ability to degrade within the body controllably. Their pathophysiological and toxicological features as well as their physical and mechanical properties, make them highly desirable as an emerging alternative for specialist applications. Magnesium is of great

interest as the primary base metal in many biomaterials, due to its extreme lightness, high fracture toughness, bone-like elastic modulus and compressive yield strength (Table 2). Further, it has a high no-observed-adverse-effect level when compared to other biodegradable metals (6.7 $\mathrm{mg\,kg_{BW}^{-1}\,d^{-1}}$ for Mg and 0.28 $\mathrm{mg\,kg_{BW}^{-1}\,d^{-1}}$ for Fe, another possible base metal[17]). Because of this, Mg is at the forefront of biodegradable metal design and is the focus of this project.

Table 2: Comparison of different biomaterials and their physical and mechanical properties. Compiled from references 2,15,16,18

Properties	Natural bone	Magnesium	Ti Alloy	Co-Cr alloy	Stainless Steel	HA[a]	Bioglass	PLLA[b]
Density ($\mathrm{g\,cm^{-3}}$)	1.8–2.1	1.74–2.0	4.4–4.5	8.3–9.2	7.9–8.1	3.1	2.5	1.21–1.43
Elastic modulus (GPa)	3–20	41–45	110–117	230	189–205	73–117	75	2.7
Compressive yield strength (MPa)	130–180	65–100	758–1117	450–1000	170–310	600	1000	-
Fracture toughness ($\mathrm{MPa\,m^{1/2}}$)	3–6	15–40	55–115	-	50–200	<1	0.7	-

[a] hydroxyapatite, [b] poly(L-lactic acid)

1.3 Chemical and Physical Characteristics of Magnesium

Magnesium is classified as an alkaline earth metal and is found in Group 2 of the periodic table (Table 3). The potential advantages of the material outlined above are counteracted by the poor corrosion and softness of the surface of Mg and its alloys.

Table 3: Atomic and physical properties of Mg. Compiled from references 18 and 19

Property	Mg
Atomic number	12
Electronic configuration	$[\mathrm{Ne}]3\,\mathrm{s}^2$
Atomic mass	$24.3050\,\mathrm{g\,mol^{-1}}$
Naturally occurring isotopes	^{24}Mg (78.99 %)
	^{25}Mg (10.0 %)
	^{26}Mg (11.01 %)
Density (20 °C)	$1.738\,\mathrm{g\,cm^{-3}}$
Electrical resistivity (20 °C)	$4.46\,\mu\Omega\,\mathrm{cm}$

1.3.1 In Vivo Corrosion Characteristics

Magnesium has the lowest reduction potential of all engineerable metals, with $E^{\ominus}_{(\mathrm{Mg^{2+}/Mg})} = -2.37\,\mathrm{V}$ vs. standard hydrogen electrode.[20]

Anodic reaction:

$$\mathrm{Mg} \rightleftharpoons \mathrm{Mg^{2+}} + 2\,\mathrm{e^-} \tag{1.1}$$

Cathodic reaction:

$$2\,\mathrm{H_2O} + 2\,\mathrm{e^-} \rightleftharpoons \mathrm{H_2} + 2\,\mathrm{OH^-} \tag{1.2}$$

In aqueous environments, Equation 1.1 and Equation 1.2 occur producing the overall corrosion process

$$\mathrm{Mg_{(s)} + 2\,H_2O_{(\ell)} \longrightarrow Mg(OH)_{2(s)} + H_{2(g)}} \tag{1.3}$$

Pourbaix diagrams provide an important graphical representation of the possible equilibrium phases of an aqueous redox system. The data is produced using thermodynamic calculations and experimentally observed behaviour. The 3-D Pourbaix diagram in Figure 2 shows that by limiting the thermodynamic activity of the surface, the equilibrium potential for the oxidation of Mg shifts positive, thus making it less thermodynamically favourable.

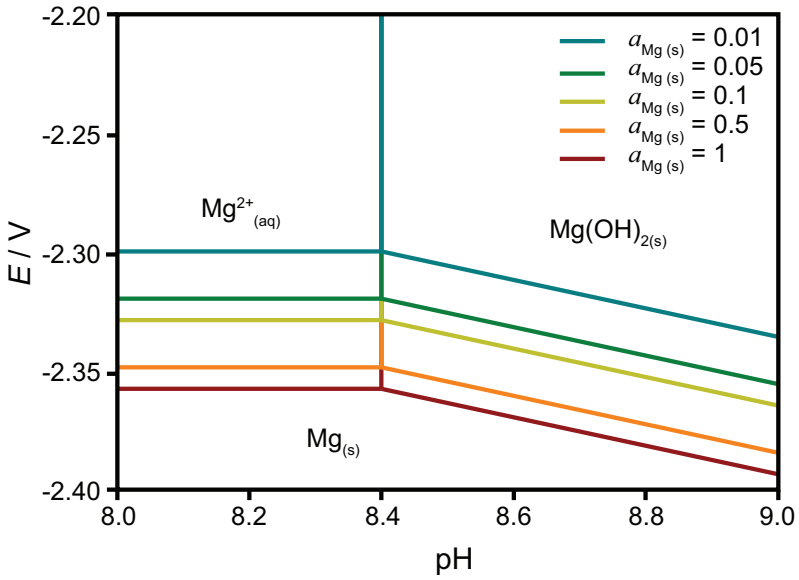

Figure 2. E-pH Pourbaix diagram for the Mg-H_2O system. The lack of MgO is due to 1.5. Reproduced from reference 21

One significant problem observed with Mg oxidation in vivo is the accompanying reduction of H_2O to form H_2 and OH^- (Equation 1.2). Zheng et al.[13] evaluated recent in vivo animal studies using Mg-based implants and reported that in approximately 70 % of cases, subcutaneous gas cavities produced by the accumulation of H_2 were observed. Due to the different H_2 solubility and diffusion coefficients in different tissues, the rate of cavity formation and hence the rate of Mg corrosion is dependent on the location of the implant,[22] with Remennik et al.[23] ranking Mg degradation in the following order: subcutaneous $>$ muscle $>$ bone. The local pH change may cause unexpected problems in vivo, however, further research on this is required.[4]

Erwin Payr is one of the most significant pioneers of the use of Mg as a biodegradable material and was able to propose that tissue O_2 and H_2O content, CO_2, the dissolved salts in blood and the chemical processes within cells were mainly responsible for the corrosion of Mg within the body.[4] Cl^- ions significantly increase the degradation rate due to the conversion of sparingly soluble $Mg(OH)_2$ to the highly soluble $MgCl_2$ (Equation 1.4).[24] Significant corrosion is typically observed when Cl^- concentrations are greater

than 30 mM and severe pitting corrosion can be observed on Mg in vivo,[17,24,25] where the concentration is about 100 mM.[26]

$$Mg(OH)_{2(s)} + 2\,Cl^-_{(aq)} \longrightarrow MgCl_{2(s)} + 2\,OH^-_{(aq)} \tag{1.4}$$

In vitro and in vivo corrosion studies are complicated by the contribution of many factors, including: ions (mainly Ca^{2+}, ${PO_4}^{3-}$, and ${CO_3}^{2-}$); biomolecules (proteins, amino acids, lipids, hormones, etc.); cell adhesion, tissue formation; and the resorption and dissolution of the implant itself. The anatomical environment also plays a significant role in controlling corrosion rates, with blood flow, pH, CO_2 and H_2 diffusion and mechanical stress being the main factors.[13] The precise corrosion morphology of Mg and its alloys depends on the chemical, physical, mechanical and environmental conditions.

1.3.2 Lowering the Corrosion Rate for In Vivo Use

Bare, pure Mg experiences a corrosion behaviour which is typically too fast for many applications and results in the formation of gas cavities and, therefore, requires modification whether by alloying or through the use of coatings.

Alloying can result in the improvement of strength and creep resistance, but the pathophysiology and toxicology of degradation products have to be taken into account.[2,13] Not only must the alloying material slow the corrosion rate, but it must remain biocompatible within the vicinity of implantation. The alloys of most interest include elements which are essential in the body ($>50\,mg\,kg^{-1}_{BW}$: Fe, Ca, Zn, and Mn), potentially essential ($<50\,mg\,kg^{-1}_{BW}$: Sr, Si, and Sn), or have proven characteristics which may be advantageous for alloying (Li, Al, Zr, Bi, and Y and lanthanides).[2] Alloys have to be carefully designed such that the phase boundaries of individual grains do not form anodic and cathodic regions which can result in accelerated degradation due to galvanic corrosion.[2] Further, the release of alloying metal ions will have a direct effect on the viability of cells and tissues in the area surrounding the implant. Significant research is still required on the in vivo corrosion characteristics of these metals and into the potential toxic effects of alloy corrosion products due to their high local concentrations.[2]

Surface modification has been shown to decrease the rate of Mg corrosion to some extent. The decrease has been reported to range from close to 20 % to over 90 % after surface modification.[13] However, obtaining uniform corrosion and coating stability remain significant problems. Microcrack and defect formation in the surface coating can result in the acceleration of local degradation.[12,13,27] Many different surface protection methods have been reported in the literature, including chemical methods such as fluoride[28] and alkali treatment,[29] electrochemical treatment,[30] bone-like mineral deposition,[31] sol-gel treatment,[32] and organic polymers coatings (polydopamine,[33] chitosan,[34] cellulose,[35] collagen,[36] gelatin,[37] poly(L-lactic acid) (PLLA),[38] poly(ε-caprolactone) (PCL),[39] and poly(lactic-co-glycolic acid) (PLGA)[40]). Mechanical techniques have also been employed, such as high-speed dry milling, ball burnishing, laser shock peening and cryogenic machining.[13] Zheng et al.[13] summarise several of these techniques, and Heise

et al.[12] give an in-depth discussion of natural polymeric coatings in vitro and in vivo. Further development of surface coatings and investigations into their biocompatibility and clinical applications will result in the design of better and more sophisticated implants. It is paramount that the surface chemistry of Mg is understood before any modification occurs.

1.3.3 Surface Structure

In air, Mg naturally forms a passivated surface layer consisting of mainly $Mg(OH)_2$ and MgO; alloying elements also form hydrated oxide components if present. MgO has a NaCl-like structure, is an excellent thermal conductor, and is a good electrical insulator. MgO is a simple basic oxide and reacts with H_2O to form a hydroxide layer (Equation 1.5). This hydroxide layer is partially soluble but can protect the surface in dry air.

$$MgO + H_2O \longrightarrow Mg(OH)_2 \tag{1.5}$$

The Pilling-Bedworth ratio (see Appendix 6.1) of $Mg(OH)_2$ to Mg (0.81[41]), shows that the hydroxide layer is porous and inadequately covers the underlying metal. Additionally, there is a mismatch between the hexagonal close-packed structure of the bulk Mg and cubic and hexagonal structures of MgO and $Mg(OH)_2$ respectively. There is a high degree of compressive strain on the passivated surface,[18] which can quickly lead to cracking which exposes the base metal to potentially corrosive substances resulting in corrosion. Commercial surface treatment of Mg often requires the use of an additional sealant.

Extensive studies by Nordlien et al.[42], Santamaria et al.[43], and Yao et al.[44] have investigated the formation of oxide films on the surface of pure Mg in dry, humid and aqueous environments using a range of analytical techniques, including X-ray photoelectron spectroscopy (XPS) and photocurrent spectroscopy (PCS). The thickness of the oxide film ranges from 20–50 nm, with a median of 25 nm[42] with an underlying MgO film 5–6 nm thick[44] and is independent of differences in grain orientations and variations in the time between cutting and observations. With exposure to H_2O, $Mg(OH)_2$ forms preferentially on the outermost layer forming a platelet structure (Figure 3a) and then grows in thickness with exposure time (Figure 3b).

The variable and poorly passivated surface is chemically and physically detrimental for the development of Mg-based materials unless significant modifications to the surface occurs. Optimal surface protection can be achieved with attention to the principles set out by Kurze:[18]

- Any errors during the processing or manufacturing will propagate, and not even the best surface protection can compensate for imperfections.
- High-purity Mg should always be used. Heavy metal impurities result in galvanic corrosion under protective coatings, forming H_2 and causing the protective coating to lift and the exposure of the base Mg to the environment.
- The porosity of the Mg should be limited as high porosity can trap electrolyte and

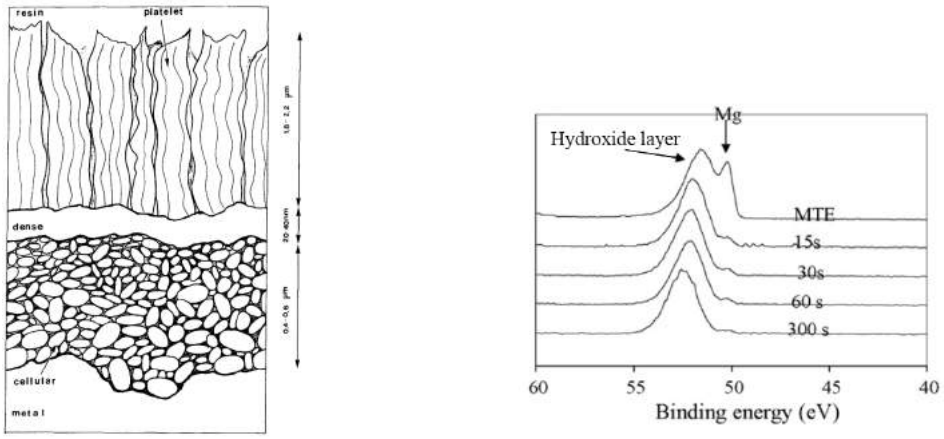

(a) **(b)**

Figure 3. Film morphology of oxide layer of Mg after exposure to H_2O. **(a)** Schematic drawing of Mg surface after exposure to aqueous solution. Reproduced from reference 42. **(b)** XPS scan of the Mg 2p region showing the disappearance of the metallic Mg peak with immersion in pure water for 15–300 s. MTE is mechanically treated electrodes. Reproduced from reference 43.

increase corrosion and release of H_2 and destroy of protective coatings.

1.4 Surface Modification via Reduction of Aryldiazonium Salts

Increasing the corrosion resistance of Mg is the primary challenge inhibiting adoption of the material in more widespread applications. Although surface modification of Mg has been achieved using a variety of techniques,[18] many surface treatments are incompatible with a biomedical application and give coatings that suffer from poor adhesion to the metal surface. It is almost impossible to get a complete compact coating by wet chemical methods because of the hydrogen bubbles generated during coating.[13]

In the application of surface science, the interest in aryldiazonium salts has undergone a quantum leap. Pinson and co-workers[45] first described the use of 4-nitrobenzenediazonium (NBD) ion as a surface modifier on a glassy carbon (GC) electrode, and in the 25 years since, it has become possible to graft aryldiazonium salts onto a variety of substrates, including carbons, metals, semiconductors and polymers.[46,47] The major pathway for grafting via aryldiazonium salts in acidic and non-aqueous media involves the reduction of the diazonium ion, followed by homolytic cleavage of the C−N bond to form an aryl radical which subsequently reacts with the substrate to form a covalent bond (Scheme 1.1a). Multilayers form via continued grafting through previous aryl groups (Scheme 1.1b).

The reduction of aryldiazonium salts can be achieved using a variety of techniques and conditions including electrochemically, by spontaneous reduction by the substrate, photochemically, and by the addition of a reducing agent.[47] Therefore, functionalisation can be tuned to the appropriate conditions suitable for the substrate. Alternatively, if the salt is not isolable, as is the case with 4-aminobenzenediazonium (ABD), in situ generation of the diazonium from the aromatic amine with sodium nitrite (in acidic solutions) or with *tert*-butyl nitrite or isoamyl nitrite (in acetonitrile solutions) allows for grafting of

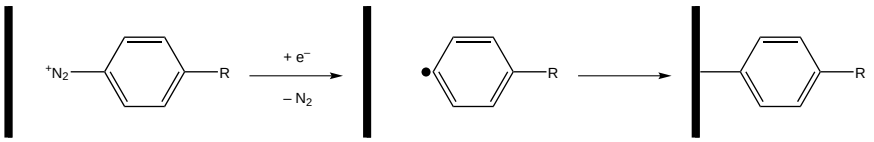

(a)

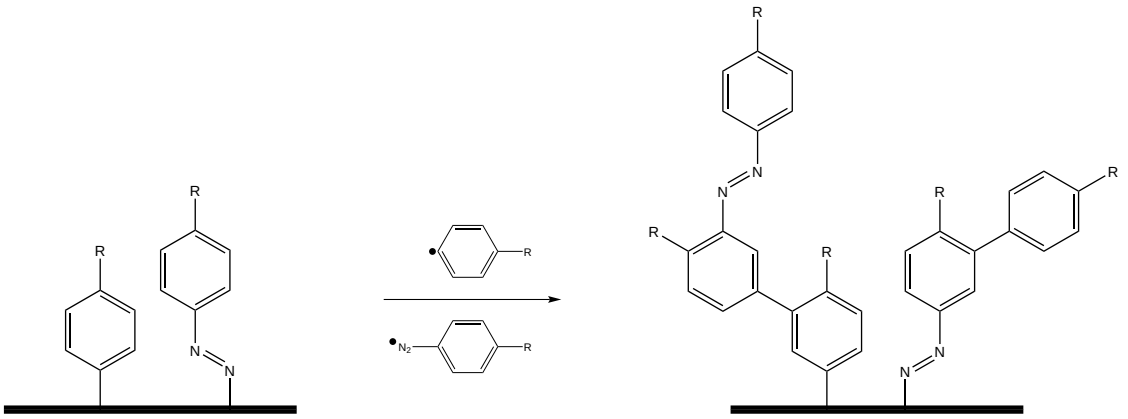

(b)

Scheme 1.1. Proposed mechanism for **(a)** reduction of an aryldiazonium ion lead to the formation of the aryl radical and subsequent reaction with a substrate; **(b)** formation of multilayers including the formation of azo linkages.

aryl groups with a broader range of functionality.

Diazonium salts are stable in aqueous acidic solution and acetonitrile, but the stability in other aprotic medium has not been systematically investigated.[46] As pH increases above pH 2-3 the stability of the ion decreases and there is rapid conversion to the diazohydroxide ($Ar-N=N-OH$) and diazoate ($Ar-N=N-O^-$) at neutral and basic pH (Scheme 1.2). However, these species are also able to form covalently grafted films on metallic surfaces.[48]

Tetrafluoroborate salts of diazonium ions are particularly advisable compared to other counter ions, such as Cl^-, as they are stable at room temperature and undergo the Balz-Schiemann reaction (Scheme A.1) upon heating.[46]

1.5 Aims

1.5.1 Overarching Goal

The overarching goal of research in this area is to develop a procedure for the chemical grafting of bioactive layers onto a Mg substrate with the aim to reduce the corrosion properties of the metal. Corrosion protection may be achieved by using a covalently attached adhesion layer which is then covalently bonded to a bioactive layer.

1.5.2 Specific Goal

The specific goal of the project is to develop and investigate the feasibility of grafting nanoscale organics layers to Mg from aryldiazonium ion solutions. The ease of preparation and a strong aryl-surface covalent bond seen on other materials suggest that the use of aryldiazonium ion grafting might be a convenient approach to give adhesion lay-

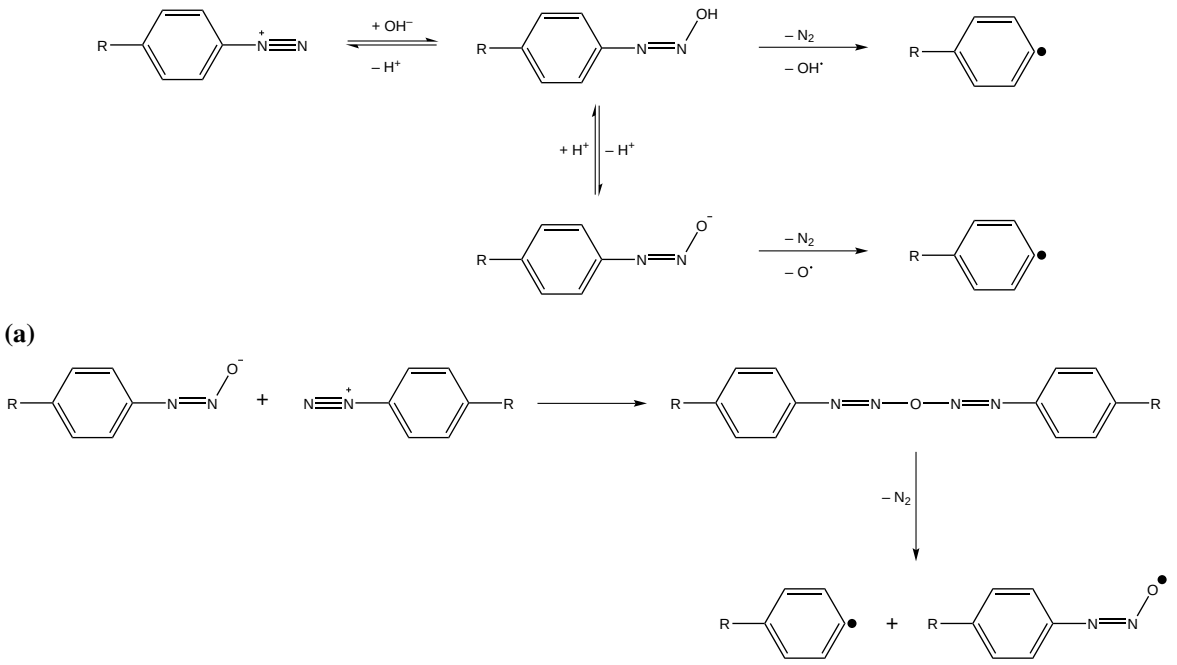

Scheme 1.2. Possible aryl radical formation mechanism in aqueous solution at pH $\geq$ 7.[48–51] **(a)** Formation of the diazohydroxide and diazoate in an alkali solution, followed by subsequent decomposition to form the aryl radical. **(b)** Formation of the oxybis(diazene) and decomposition resulting in aryl radical formation.

ers on Mg. The functionalisation of the diazonium ion will allow for several methods of coupling a second corrosion protection layer.This will be achieved by examining the reaction of 4-nitrobenzenediazonium and 4-ethynylbenzenediazonium with Mg in various media. For the most promising conditions, the procedure for obtaining strong coherent thin films will be optimised. The corrosion protection properties of the film will also be investigated.

2 Experimental Methods

2.1 General Synthesis and Reagents

2.1.1 Reagents and Solvents

All solvents and reagents were obtained from commercial sources and used as received. Non-aqueous solutions were prepared in HPLC grade solvents, and aqueous solutions were prepared in Milli-Q water (resistivity $> 18\,\mathrm{M\Omega\,cm}$).

2.1.2 Aryldiazonium Salts

Unless stated otherwise, all aryldiazonium salts used in this project have been previously reported and were prepared according to a literature method.[52] Briefly, the aromatic amine derivative (5 mmol) was dissolved by the slow addition of 25 % hydrofluoroboric acid (HBF_4, 5 mL) while stirring in an ice bath. A cold solution of sodium nitrite (5 mmol) dissolved in minimal water (1 mL) was added drop-wise while stirring for 20 min. The crude product was filtered under suction. The product was dissolved in a minimal amount

of acetonitrile (ACN) in an ice bath and gradual addition of diethyl ether re-precipitated the purified product which was filtered and washed with cold diethyl ether. The product was dried under vacuum and stored in the freezer in the dark.

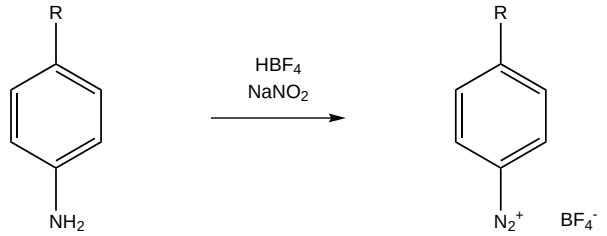

Scheme 2.1. Synthesis of an aryldiazonium salt from an aryl amine in aqueous solution.

2.1.3 Buffer Solutions

Buffers were prepared using the Henderson-Hasselbalch equation to estimate the amount of each reagent (Equation 2.1), where pK_a corresponds to the $-\log_{10} K_a$ where K_a is the acid dissociation constant, $[HA]$ is the concentration of the acidic component and $[A^-]$ is the concentration of the conjugate base.

A 0.1 M phosphate buffer (PB) was used for solutions with pH = 8, with NaH_2PO_4 as the source of acidic $H_2PO_4{}^-$ (p$K_a = 6.86$) and Na_2HPO_4 as the source of basic $HPO_4{}^{2-}$ and NaOH added to give the desired pH.

A 0.1 M carbonate buffer (CB) was used for solutions with pH = 10. NaOH was added to $NaHCO_3$ ($HCO_3{}^-$, p$K_a = 10.33$) to prepare the buffer.

$$\mathrm{pH} = \mathrm{p}K_a + \log_{10}\left(\frac{[A^-]}{[HA]}\right) \tag{2.1}$$

2.1.4 Solution for Corrosion Testing

The corrosion testing medium was prepared using 0.1 mM NaCl and 0.1 mM 2-(4-(2-hydroxyethyl)piperazin-1-yl)ethane-1-sulfonic acid (HEPES) and adjusted to pH 7.4 using NaOH.

2.2 Surface Preparation and Modification

2.2.1 Preparation of Mg Surfaces

Mg surfaces were polished successively with 400 (P800, 22 µm), 600 (P1200, 15 µm), and finally 1200 grit (P2500, 8 µm) silicon-carbide (SiC) polishing discs (Buehler CarbiMet), followed (if required) by polishing using oil-based diamond suspensions, with particle sizes of 9 µm and 3 µm (Buehler MetaDi Supreme Suspension). Samples were ultrasonicated in ethanol for 10 min, twice, before drying under a stream of N_2 and stored in a vacuum desiccator. NaOH pretreatment (PT) consists of soaking substrate in 2 M NaOH bath for 30 min at 80 °C.

2.2.2 Spontaneous Grafting of Aryldiazonium Salts

Spontaneous grafting of surface coatings was achieved by placing the polished Mg surface into a beaker with the addition 10 mL of the required aryldiazonium salt solution

(concentration and solvent as specified in the text). The beakers were then placed on an orbital shaker for the desired amount of time (1–24 h). This procedure was carried out in darkness to avoid photochemical reduction of the diazonium ion. After grafting, substrates were ultrasonicated in the same solvent that they were grafted in, minus the diazonium salt, for 5 min, followed by ethanol and Milli-Q water if required. Samples were dried under N_2 and stored in a vacuum desiccator. Control samples were prepared by following the same procedures as above, but with the immersion of Mg samples in solutions absent of diazonium salts.

2.3 Instrumental Methods

2.3.1 X-ray Photoelectron Spectroscopy

XPS data were obtained using a Kratos Axis Ultra DLD spectrometer equipped with a monochromatic Al K_α source operating at 100–150 W. Survey scans were recorded with a step size of 1 eV and pass energy of 160 eV; for narrow scans, the corresponding parameters were 0.1 eV and 20 eV, respectively. Peak fitting procedures and data analysis were conducted using CasaXPS software.

2.3.2 pH Meter

pH values were measured using an EDT Instruments GP 353 ATC pH meter.

2.3.3 Fourier Transform-Infrared Spectroscopy

FT-IR spectra were recorded using a Bruker Vertex 70 spectrometer operating OPUS software using a Bruker PLATINUM diamond ATR accessory. Mid-IR spectra were recorded using 64 scans at 4 cm^{-1} resolution from 600–6000 cm^{-1} with a liquid N_2 cooled HgCdTe detector.

2.3.4 Water Contact Angles

Water contact angles (WCAs) were measured using drops of 1 µL Milli-Q water. At least 5 separate spots were measured for each sample. Images were analysed using the low-bond axisymmetric drop shape analysis (LBADSA) method of Stalder et al.[53]

2.3.5 Electrochemistry

For all electrochemical methods, the Mg substrate was the working electrode. A copper plate pushed into the non-polished surface was used as the electrical contact for the electrode. The exposed area of the surface was 1.1 cm^2. A Ag/AgCl/3.0 M KCl reference electrode was used for electrochemical measurements; all potentials in this report are quoted against this reference. The counter electrode used in this report was a Pt mesh sealed in glass.

Electrochemical measurements were performed using an Eco Chemie Autolab PGSTAT302 or PGSTAT302N potentiostat running Autolab NOVA versions 1.11. All electrochemistry was obtained in non-deoxygenated solutions. For electrochemical corrosion testing, linear sweep voltammetry (LSV, either 10 $mV\,s^{-1}$ or 1 $mV\,s^{-1}$) were measured in a three-electrode setup over the range from -3 V to -1 V vs. Ag/AgCl. A solution

volume of $\sim 50\,\text{mL}$ was used and was replaced after every sample. Tafel plots (plots of log|current density| vs. potential) were generated by the potentiostat software.

3 Results and Discussion

There have been no published reports of covalent grafting of aryl groups to Mg. However, aryldiazonium salt chemistry has been applied to a wide range of surface types.[46,47] Previous work in this group by summer student Craig Melton suggested that aryldiazonium grafting to Mg deserved further investigation.[54]

Two different diazonium ions were investigated during this work: 4-nitrobenzenediazonium (NBD) and 4-ethynylbenzenediazonium (EBD). NBD is the benchmark for work involving diazonium ions due to its well behaved and well-documented grafting procedures and its high stability when compared to other diazonium ions. The $-NO_2$ tag is detectable by many spectroscopic techniques including XPS and IR spectroscopy. The $-NO_2$ group can undergo reduction group to an amine by several methods, allowing for further modification of the surface to occur. Another critical feature for the use of NBD is its ease of reduction to the aryl radical which occurs in a variety of media and can occur spontaneously, electrochemically, or photochemically. EBD is also easily reduced. Furthermore, the presence of the presence of the $-C\equiv C-H$ function group expands the possible routes for additional layer functionalisation using click chemistry.

The spontaneous formation of the aryl radical and simultaneous grafting to a surface is typically achieved in ACN or acidic aqueous solution (pH ≤ 3), however grafting in neutral or basic conditions can also result in film formation (Scheme 1.2). The pH of the medium for spontaneous grafting to Mg requires consideration, as Mg will undergo corrosion at a pH below 8.4 (Figure 2). In this work, grafting was initially done in pH 8 and 10 aqueous PB and CB respectively, and subsequently in unbuffered Milli-Q water and ACN. Although it would be expected that Mg will corrode in the pH 8 solution, previous work by Melton et al.[54] appeared to show grafting at this pH.

3.1 Buffered Aqueous Solutions

3.1.1 Phosphate Buffer Solution

Table 4 details the experimental procedures and observations for the grafting of NBD and EBD and controls in PB. Photographs of surfaces are shown in the Appendix Figure A.1 to Figure A.3. With the control samples (samples 'reacted' in the absence of diazonium salt), crystals form on the surface of Mg. The insoluble Mg phosphate salts ($Mg(H_2PO_4)_2$, $MgHPO_4$, and $Mg_3(PO_4)_2$) are the probable cause for these crystallites. Localised degradation on the surface produces Mg^{2+} which then precipitates as the phosphate salt.[55] Sonication does not remove the crystals indicating that they are held tightly by the $Mg(OH)_2$ layer.[13] Deposition of phosphates and calcium salts is also observed when pure Mg is exposed to in vivo environments.[56] Substrates modified for 24 h, with or without NaOH pretreatment, show high concentrations of crystal growth. When exposed to PB for a shorter period of time (1 h) the rate of degradation at high pH is slow enough

that significant crystal growth cannot occur.

Samples modified with NBD show a range of surface morphologies, but all suffer from uncontrollable film growth. Samples modified for a significant amount of time have a thick layer after removal from the modification medium, which undergoes complete or partial destruction upon sonication. The surface morphology of samples exposed for a shorter period or use of NaOH pretreatment are more controllable, although the surface layers are incomplete. Bubble formation and corrosion caused by the solution during modification are assumed to block the grafting of the aryl radical to the surface.

Grafting of EBD is significantly more reproducible when compared to NBD but still suffers from problems. Modification using EBD results in a film which provides a uniform coating, albeit with small perforations due to the presence of bubbles on the surface. However, compared to NBD modification the surface coating is attached solidly to Mg, with destruction not occurring upon sonication.

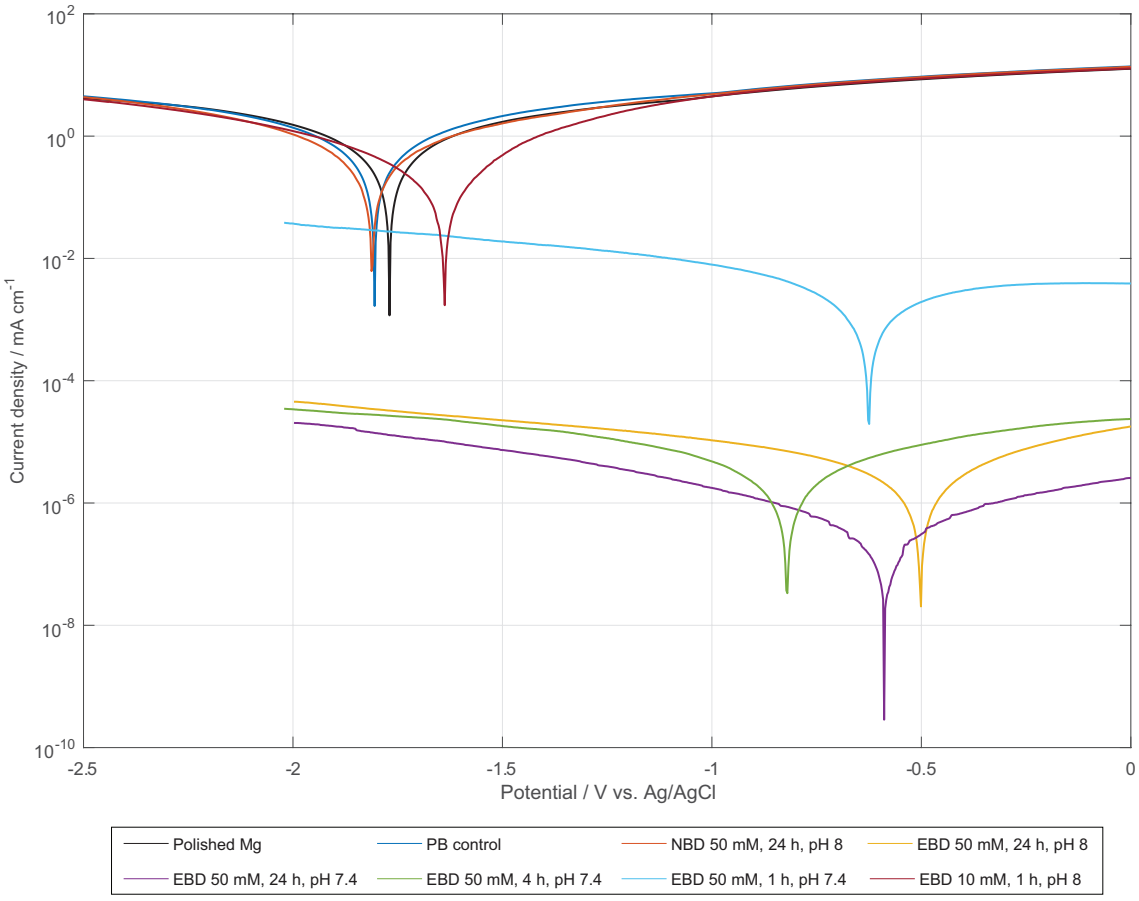

Figure 4. Tafel plots of polarisation curves of substrates modified in PB. LSV scanned at a rate of $10\,\mathrm{mV\,s^{-1}}$.

Table 4: Overview of the experimental procedures and the observations of the solution and the substrate after reaction of Mg with NBD and EBD, and for control samples.

Diazonium	Conditions[a]	Solution Appearance	Sample Appearance	Comments	Fig.[b]
None (control)	pH 8, 24 h	Bubbles form on the surface, no visual change to the solution.	Crystallisation has occurred on the surface. Mg phosphate salts are the probable cause for these crystallites. Gas bubbles also present on surface		A.1a
	pH 8, 1 h	As above	Beginning of crystallisation of the surface, although the polish of the surface is still visible		A.1b
	NaOH PT, pH 8, 24 h	As above	Significant crystallisation observed on surface		A.1c
	NaOH PT, pH 8, 1 h	As above	The surface appears duller, although not consistent over the entire surface. Small crystals form. No visible polished metal underneath.		A.1d
NBD	pH 8, 50 mM, 24 h	Forms a thick brown precipitate which has trapped bubbles. Solution colour on it own is brown/orange	Before sonication there is a thick brown layer on the surface, however, after sonication, this layer breaks down leaving the bare Mg.	Films were patchy, and reproducibility was poor.	A.2a
	pH 8, 50 mM, 1 h	A brown precipitate formed as above, but the layer was thinner.	After sonication surfaces were uniformly covered in a thick (visible) orange-brown colour layer	For this time, samples seemed to be better controlled and reproducible. Sonication did not remove the layer.	A.2b
	NaOH PT, pH 8, 50 mM, 24 h	Brown precipitate formed as above and solution discolouration	Thick brown layer coats the centre and becomes thinner towards the edges. Irregularities in the coatings in certain places are likely due to bubble formation	Not very consistent between samples.	A.2c
	NaOH PT, pH 8, 1 mM, 24 h	A brown precipitate formed as above, thinner than above	Orange-brown coating dotted with the locations where bubbles had formed in solution		A.2d
EBD	pH 8, 50 mM, 24 h	A thick brown solution formed, precipitate floated about in slightly orange coloured solution	Very thick brown layer, small holes due to gas bubbles. Cracks appear on the surface after corrosion testing but remains attached to surface.		A.3a
	pH 7.4, 50 mM, 24 h	as above	Thick brown surface, with darker marks near edges of surface	Surfaces on two samples peeled off after sonication (Figure A.3c), but one had the same appearance as above.	A.3b
	pH 7.4, 50 mM, 4 h	As above	Film completely covers surface and edges of substrate, albeit with holes	Very reproducible method.	A.3d
	pH 7.4, 50 mM, 1 h	As above	Thinner than above layer, but still uniformly distributed across substrate and with small holes which appeared after sonication		A.3e
	pH 8, 10 mM, 1 h	Solution was orange coloured and becoming more opaque bubbles had formed around the edges of the sample and at the top of the solution	Visually thinner surfaces than above and the coating is cracked at the edges of the surface but otherwise uniform coating.		A.3f

[a] NaOH pretreatment (PT, if used), solution pH, concentration of diazonium salt if present, immersion time of the sample in solution.

[b] Photographs of surfaces are shown in the Appendix Figure A.1 to Figure A.3.

3.1.2 *Corrosion Testing of Phosphate Buffer Substrates*

The corrosion resistance of the newly grafted aryl layers was investigated using polarisation curves and visualised as Tafel plots (Figure 4). In Tafel plots, the potential of the minimum current corresponds to the corrosion potential (E_{corr}) and the current density (j) over the higher potential range indicates the rate of Mg oxidation, while over the lower potential range indicates the rate of H_2 generation by H^+ reduction. Extrapolation of the two arms using the Tafel equation yields the exchange current density (j_0). Comparing the Tafel plot for a polished-only Mg substrate (black line) with a PB control (blue line) and NBD modified sample (orange line), we see there is no significant improvement in the corrosion resistance with any treatment (j_0 are very similar), indicating that neither the crystals on the control nor the nitrophenyl film provide protection to the surface. This was also seen in repeat experiments, indicating that the use of NBD does not provide corrosion protection and would require the use of a second coupled layer for this purpose. Contrarily, EBD shows a large positive shift in E_{corr} of about 1.5 V and j_0 decreases by a factor of up to 10^6 times. Longer reaction times were observed to produce the most corrosion resistant surfaces, coming from samples which had a visibly thicker coating. Shorter grafting times still decrease the current significantly presumably due to a thinner film.

Although the surfaces modified with EBD show excellent corrosion resistance, the poor stability of the coating on all the substrates measured resulted in the coating cracking and in some cases completely detaching from the surface after electrochemical testing (Figure 5).

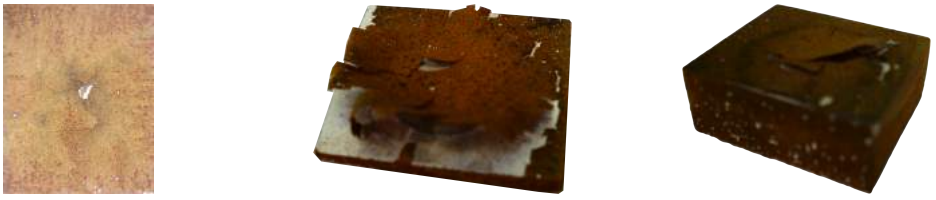

(a) **(b)** **(c)**

Figure 5. Cracking and dissociation of EBD film after electrochemical corrosion testing. Sample modification follows: **(a)** 25 mM in pH 8 PB; **(b)** and **(c)** 10 mM in pH 7.4.

One possible reason for the destruction of the coating is that, due to the formation of microcracks and imperfections during the reaction stage, during corrosion testing the corrosion medium can dissolve the underlying metal Mg. This is a common corrosion failure mechanism of coated Mg-based materials.[12]

3.1.3 *Carbonate Buffer Solution*

At the pH of PB solution (pH 8), corrosion of Mg will occur in solution, however, a coating on Mg using EBD was able to form from this solution. To investigate whether pH had any impact on the surface, a pH 10 CB was used as the modifying medium. A coating on Mg using EBD was successfully achieved in PB but disintegrated after testing

electrochemically, so the use of a higher pH solution would hopefully inhibit corrosion of Mg during the grafting stage, allowing for a stronger film to form.

(a) **(b)** **(c)**

Figure 6. Mg substrates after exposure to CB for 24 h. **(a)** control before sonication; **(b)** control after sonication; **(c)** after reaction in 50 mM EBD solution and sonication.

In CB, the surface of the Mg control develops a dark matte coating due to the insolubility of $MgCO_3$ (Figure 6a). However, unlike the crystallisation formed in PB, this coating disappeared after sonication, revealing corrosion had occurred (Figure 6b). EBD modification on Mg resulted in a thick brown surface, not unlike the surfaces developed using PB, however, upon sonication in CB the film completely disintegrated and eventually resulted in the surface seen in Figure 6c. Large pores and discolouration to the surface are seen.

3.1.4 Corrosion Testing of Samples Prepared in Carbonate Buffer

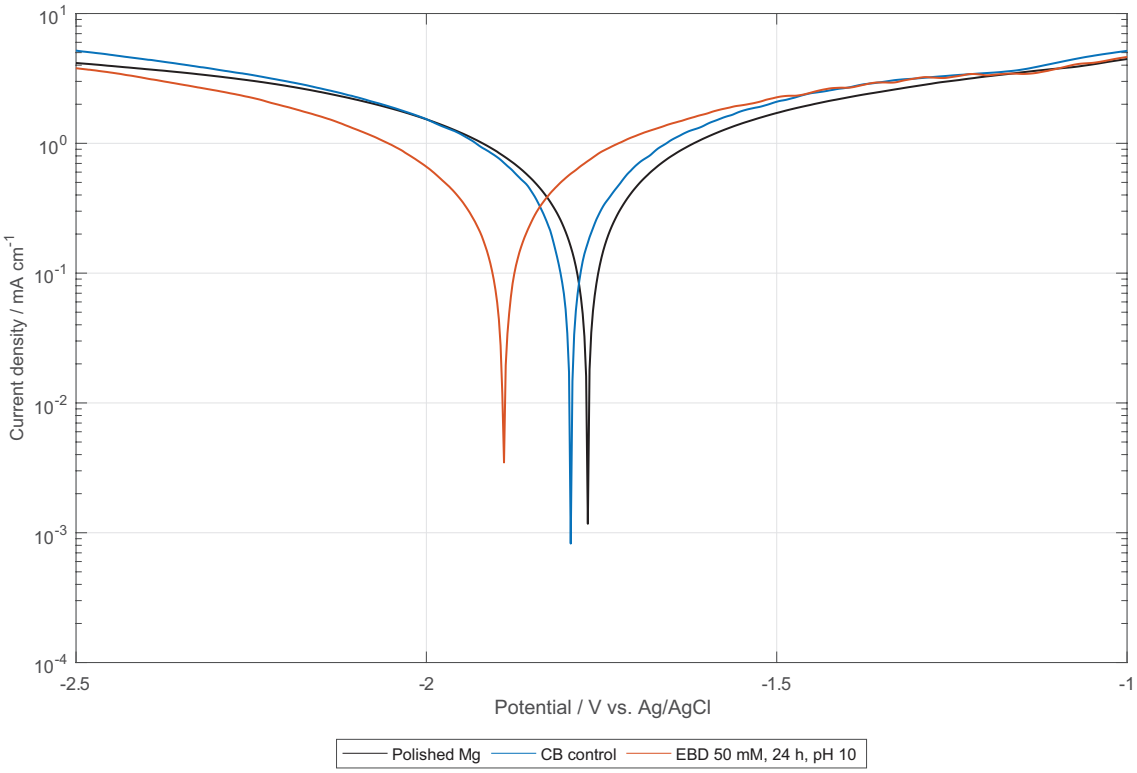

Figure 7. Tafel plot of polarisation curves of substrates modified in CB. LSV scanned at a rate of $10\,\mathrm{mV\,s^{-1}}$.

Corrosion testing of the EBD modified surface reveals a small negative shift in E_{corr}. This shift is within the range of sample to sample variability. Evidently, there are no sig-

nificant changes to the corrosion properties of the substrate when compared to a polished Mg surface.

3.1.5 Buffer Solution Summary

The use of a buffered solution as the medium for reduction of the aryldiazonium ion to the aryl radical and spontaneous grafting to Mg was to limit simultaneous corrosion of the surface. EBD was able to reproducibly form thick, macro-scale films that significantly improved the corrosion resistance of Mg. Additionally, EBD film thickness was dependent on modification time and the concentration of the diazonium salt, possibly allowing for future controllability and tunability with EBD-based films. A significant problem was film stability: electrochemical measurements resulted in the formation of cracks and even the complete detachment of the film, something which would undoubtedly require improving if further research is to be done using EBD.

Although NBD is the benchmark for aryldiazonium ion chemistry, significant problems were observed with its grafting to Mg. Although coatings formed on Mg, sonication was able to partially remove the aryl layer exposing the bare metal underneath. This would indicate that NBD does not thoroughly coat the underlying Mg and could not be an effective adhesion layer.

Even though EBD grafting was able to give a corrosion protecting layer on Mg, the aim for the aryl layer was to enable further coupling of a bioactive layer such as chitosan or cellulose. The physical thickness of the coating is a concern when biodegradability is taken into account. Any coating on Mg will be required to completely break down within the body, but such a thick coating may not be able to do this, potentially leading to severe complications in vivo. Additionally, phenylacetylene, the product of substitution of the $-N_2^+$ with hydrogen, is a suspected carcinogen[57] and it would be expected that a thick film of this and related compounds would have carcinogenic properties. Limiting the thickness of this film to the minimum required to enable grafting of a bioactive layer would reduce the possibilities of further unwanted complications. Because of these limitations, further work looks at the development of aryl layers which are thin.

3.2 Thin Layers

A new approach was required to investigate the growth of thin films. The presence of phosphate and carbonate ions in buffer solution was detrimental to the development of aryl layers to the Mg surface. In aqueous solutions, local galvanic corrosion can occur, and the resulting Mg^{2+} ions precipitate back as a salt. Ultra-pure Milli-Q water and ACN were used as the grafting media instead of buffered solutions. Table 5 overviews the reactions investigated throughout this section and photographs of the Mg surfaces can be found in Appendix Figure A.4 to Figure A.6. Milli-Q water has a pH of approximately 6.4 which indicates that corrosion can occur in the medium as is seen in Appendix Figure A.4a, however, due to the lack of added salts, no crystallisation on the surface is observed. By limiting the reaction time, corrosion is not significant compared to that in the previously used buffer media.

ACN is a commonly used medium for diazonium salt chemistry as diazonium ions are stable in it, meaning grafting occurs via the pathway shown in Scheme 1.1. Furthermore, Mg does not corrode in ACN, meaning simultaneous redox reactions are not a concern while grafting. Finally, a greater range of diazonium salts can dissolve in ACN compared to H_2O.

With two exception, use of both water and ACN and NBD for grafting result in no visual changes to the surfaces when reacted for 4 h. The first exception is the substrate modified using 1 mM NBD in H_2O which gained an orange coating (Appendix Figure A.6a). For reactions in water, in contrast to the control samples, no corrosion is observed on diazonium ion surfaces after 4 h, indicating that there is some corrosion protection resulting from the presence of the diazonium ion. This tells us that the diazonium ion is at least physisorbed to the surface and blocks the solution corrosion. However, what is very interesting is the discolouration which occurs using a low (1 mM) but not high (10–25 mM) concentration of NBD to modify Mg. The lower concentration appears to give the formation of a layer not unlike that formed when using a buffered solution. One possible reason for this is that, in the higher concentration solution, the diazonium ion grafting blocks the surface and prevents corrosion, while the 1 mM solution leads to too little grafting to adequately protect the surface, allowing a small amount of corrosion to occur. Nordlien et al.[42], Santamaria et al.[43], and Yao et al.[44] all report that the thickness of the surface $Mg(OH)_2$ layer increases when exposed to H_2O. In the 1 mM NBD solution, as the $Mg(OH_2)$ layer thickness increases, the rate of electron transfer from the metal to the diazonium ion in solution decreases, decreasing the rate of formation of the aryl radical. With electron transfer from the surface blocked, the diazonium ions react with each other, radicals (formed from thermal decomposition), or other decomposition products in situ before precipitating onto the Mg surface. The colour of the surface likely comes from the azo products which usually highly coloured. The different outcomes described here of reactions of 1–25 mM in water were reproducible.

The second exception is the substrate modified using EBD (at 10 mM and 25 mM) in water. Both samples react immediately upon the addition of the diazonium ion solution, forming a orange coating on the Mg surface. Formation of bubbles was also observed rapidly, but had subsided after 4 h. The sample modified with concentration of 25 mM lost the coating during sonication.

The reactivity of the diazonium ion in solution may result in these ions coupling in the bulk solution before precipitating from solution onto the surface. The rapid reaction rate indicates that the presence of Mg promotes this reaction, meaning electron transfer from the surface likely occurs before a thick hydroxide coating inhibits this. The blocking of electron transfer is also seen with 1 mM NBD solution reacting with water, so it is reasonable that this could also occur here. Since these coatings are not on the nanoscale, they were not analysed further, but investigations into the formation of these films is undoubtedly required.

Table 5: Overview of the experimental procedures and the observations of the solution and substrate after reaction of Mg with NBD and EBD and for control samples in Milli-Q water and ACN.

Diazonium	Solvent	Concentration (mM)	Solution observations	Surface observations	Comments	Fig.[a]
None (control)	H_2O		Bubbles form in solution and around the Mg substrate, otherwise no visible changes to solution	Sample loses mirror polish, forming matte corrosion product layer		A.4a
	ACN		No visible changes to solution	No visible changes to surface		A.4b
NBD	H_2O	1	Solution changes from a weakly orange solution to a dark brown solution.	Surface forms evenly dispersed brown coating which does not sonicate off		A.5a
		10	Solution appears to become a slightly deeper shade of yellow/orange	Visually there is no change to the surface		A.5b
		25	Solution appears to become a slightly deeper shade of yellow/orange	No visible change to the surface	Polished to a finer standard. Samples prepared for XPS were sonicated in H_2O to remove excess carbon-based solvents	A.5c
	ACN	25	Solution appears to become a slightly deeper shade of yellow/orange	No visible change to the surface	Samples prepared for XPS were sonicated in H_2O to remove excess carbon-based solvents	
EBD	H_2O	10	Fine bubbles are produced from surface initially but subside by the end of the 4 h. Solution turns a deeper shade of yellow-orange	Surface forms a brown coating, although not as thick nor as quickly as the 25 mM sample. Coating remains intact after sonication.		A.6a
		25	Bubbles form almost instantly, and solution darkens to a yellow-orange colour	The surface on Mg discolours instantly forming a thick brown coating. Sonication removes this layer revealing the underlying metal		A.6b
	ACN	10	Solution turns a darker yellow	No visible differences		A.6c
		25	Solution turns a darker yellow	No visible differences		A.6d

[a] Photographs of surfaces are shown in the Appendix Figure A.5 to Figure A.6.

3.2.1 Water Contact Angles (WCA) of 4-Nitrophenyl Grafted Surfaces

With the exception of the sample prepared in an aqueous solution of 1 mM, none of the samples prepared in water of showed visually detectable surface layers, Further investigations were undertaken to examine whether grafting had indeed taken place. A change in the surface free energy of a solid can have a fundamental impact on the measured contact angles. WCAs were measured on control and 'modified' samples and the results are shown in Table 6 and Figure 8. The WCA on a clean freshly-polished Mg plate is $57 \pm 2^{\circ}$, indicating that the surface is hydrophilic.[58] Exposure to H_2O produces a super-hydrophilic surface with the droplet spreading to give a near-zero contact angle. This is likely due to a change in the topography of the surface with increasing roughness and the increase in thickness of the hydrophilic $Mg(OH)_2$ layer.[43] When reacted with NBD, all samples show a significant increase in WCA compared with the control sample. A WCA of close to 60–80° is often reported for 4-nitrophenyl (NP) films grafted to other surfaces and is consistent with the chemical nature of NP groups.[59] However, when compared to the freshly polished surface, the 1 mM sample becomes more hydrophilic, 10 mM shows no change and 25 mM increases in hydrophobicity. The above description concerning the development of the coloured film for the 1 mM modified surface agrees which the results seen here, as a thicker $Mg(OH)_2$ layer would also increase the wettability of the surface as seen with the control. For the sample reacted in 10 mM NBD solution, the concentration of NP on the surface may have a surface free energy approximately equal to that of bare Mg resulting in little change to the WCA, however, it is clear that the presence of the diazonium protects the surface from corrosion while grafting occurs as no corrosion is visible. An increase in the WCA for the substrate modified with 25 mM NBD sample indicates that modification of the surface free energy of the Mg substrate has occurred, and the presence of a NP film on the surface.

The transition from a hydrophilic metallic surface to a more hydrophobic character upon aryl grafting is a general trend observed on many materials and is not unexpected on Mg.[60] WCA shows that the grafting of NP group to Mg has likely occurred. Determination of surface properties such as roughness, heterogeneous composition and charge will require further investigation and calculations of surface energies and contact angle hysteresis.

Table 6: WCA measurements for polished Mg, a Mg control sample and substrates reacted with NBD in water at various concentrations for 4 h.

Sample	Contact angle (°)	$\pm\sigma$ (°)	Fig.
Polished Mg	57	3	
Control	10	1	
1 mM	49	3	8a
10 mM	56	3	8b
25 mM	69	5	8c

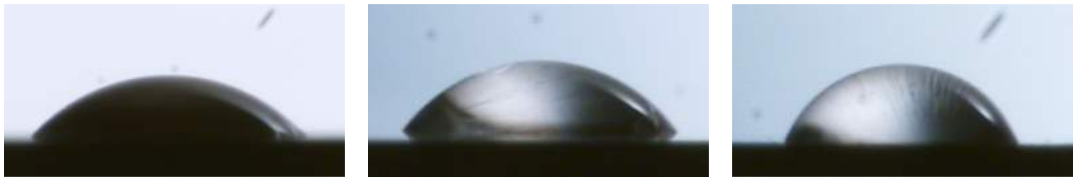

(a) **(b)** **(c)**

Figure 8. WCA pictures for Mg substrates modified with NBD for 4 h. Samples modified in solutions with NBD concentrations of **(a)** 1 mM; **(b)** 10 mM; and **(c)** 25 mM.

3.2.2 Infrared Spectroscopy of 4-Nitrophenyl Grafted Surfaces

The IR spectra of modified Mg surfaces provides complementary information to the XPS and WCA results and is a powerful tool for film analysis. Figure 9 shows the spectra for Mg substrates reacted with NBD, and Table 7 contains assignments of peaks. The symmetric and asymmetric NO_2 vibrations in the NBD spectrum are intense peaks at 1317 cm^{-1} and 1540 cm^{-1} respectively (Figure 9 (A)). These vibrations are shifted to 1350 cm^{-1} and 1524 cm^{-1} respectively upon grafting. Nitro vibrations are sensitive to aryl substitutions, such that this shift could indicate the formation of a film. It is clear that the reaction with NBD gives a significant amount of NP film at the interface including prepared in 1 mM NBD solution.

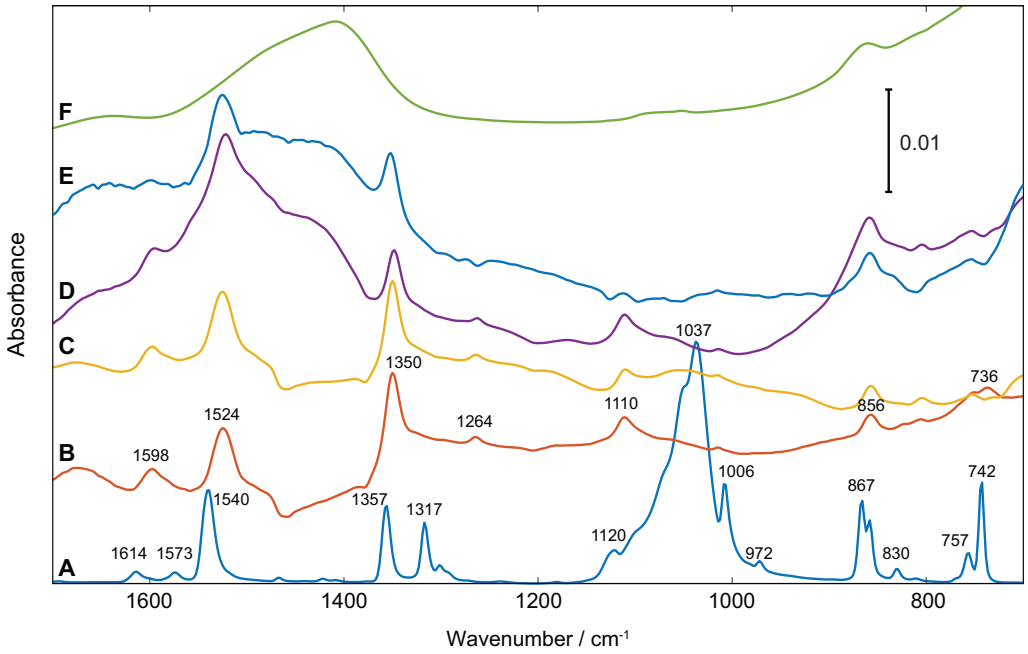

Figure 9. IR spectra of (A) $NBDBF_4$, scaled by 0.05; (B-D) Mg reacted in water with NBD with concentration: (B) 25 mM, (C) 10 mM, (D) 1 mM; (E) Mg reacted with 25 mM NBD ACN solution; (F) water control. All samples modified for 4 h. Spectra were collected in ATR mode and are offset for clarity.

However, the sample reacted with 1 mM in water (D) and the sample reacted with 25 mM in ACN (E), show the emergence of a broad peak at approximately 1410 cm^{-1}, indicative of the formation of corrosion products also visible in sample (F), the water

control. As explained above the presence of corrosion products in sample (D) is not a surprise. After the reaction in 25 mM ACN solution, sample (E) was sonication for a third time in H_2O to remove any excess organic solvent which possibly caused corrosion to occur simultaneously. Possible solutions to this may involve sonicating for a shorter amount of time or only washing the surface and drying immediately afterwards.

No peak in the N_2^+ vibrational region (2250–2350 cm^{-1}) was observed for modified surfaces (Appendix Figure A.7), indicating unreacted diazonium groups are absent, as well as indicating the major pathway for grafting occurs via the nitrophenyl radical. Azo linkages are only weakly IR active and were not observed in the spectra.

Summarising the spectroscopic data, there is clear evidence of NP film formation on the surface of Mg. By altering the concentration of diazonium salt in the grafting solution, the intensity of the NO_2 peaks increases with concentration and at a too low of a concentration corrosion on the surface occurs.

Table 7: Assignments of infrared vibrations appearing in Figure 9. Tabulated from references.[61–64]

NBD	NP-Mg	Assignment
2306 s		$-N\equiv N^+$
1614 m, 1573 m	1598 m	ν (C=C)
1540 vs	1524	ν_a (NO_2)
1467 w		Ring def + C–H wag
1421, 1409 w		ring def modes
1357 vs	1350	ν_s (NO_2)
1317 vs		ν_a (NO_2) + ring mode
	1264 m	
1120 m, sh	1110	ν (C–NO_2) + C–H wag
1037 vs		BF_4^-
1006 m, sh		CH in-plane bend
867 s, 757 m, 742 s	867	CH out-of-plane bend
858 m, sh		C–NO_2

3.2.3 X-ray Photoelectron Spectroscopy of NBD Modified Surfaces

XPS data in an invaluable technique to investigate the surface characteristics of substrates and the results reported above show the formation of nanoscale films onto the surface. XPS characterised the surface chemical composition of modified and unmodified Mg substrates. All spectra were calibrated by assigning the binding energy of the aliphatic carbon (C–C and C–H) to 284.8 eV. Samples were neutralised to account for charge accumulation on the surface. From the survey spectra (Figure 10) we can determine the atomic ratio of elements on the surface (Table 8).

All samples have a significant amount of C, including the polished Mg and control samples. Adventitious carbon is always present as a contaminant in XPS measurements, and it is clear that the polished sample is partially contaminated. This sample will not be

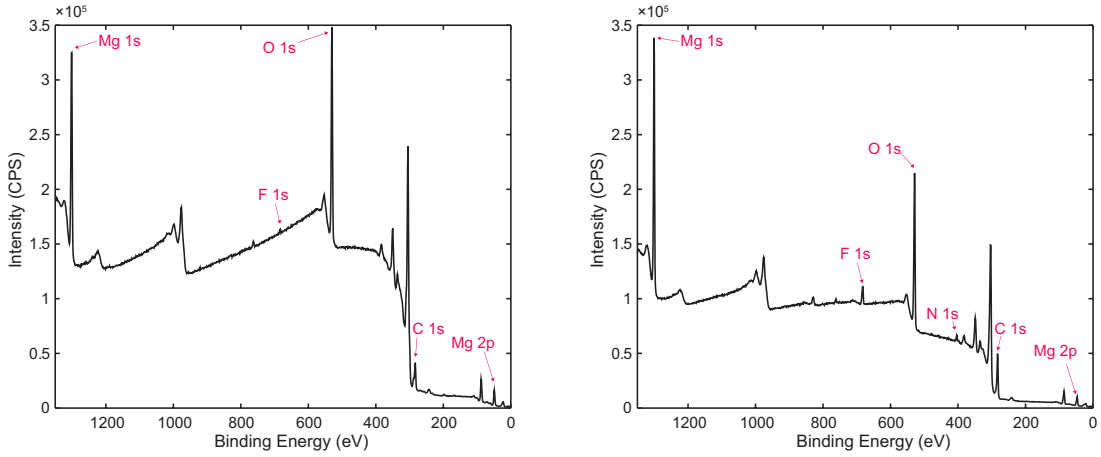

Figure 10. XPS survey spectra of along with peak assignment.[58] **(a)** polished Mg, **(b)** Mg modified with NBD in ACN. All samples modified for 4 h and NBD concentration of 25 mM. Survey scans for other samples can be found in Appendix Figure A.8.

discussed further.

Comparing the two modified samples with their respective controls, there is a higher percentage of C on the modified samples, and the O:C ratios are smaller for the modified samples indicating that less oxide film forms on the modified samples. This ratio is lowest for the sample modified in ACN, consistent with minimal corrosion in this medium. The controls and modified samples all have N present, but there is significantly more on the modified samples consistent with the expected NP film. N on the controls is attributed to adventitious contamination. Similarly, there is a small amount of F arriving from adventitious contamination, except for the sample modified in ACN where the relatively large amount may suggest some BF_4^- (the counter ion in the diazonium salt) or F^- is present.

Table 8: Atomic composition of Mg surface for polished Mg; H_2O control; Mg modified in water with 25 mM NBD; ACN control; Mg modified in ACN with 25 mM. All samples modified for 4 h.

Sample	Atomic %				
	Mg	C	N	O	F
Polished Mg	19.4	26.8	-	53.3	0.5
H_2O control	29.3	14.1	0.9	55.6	0.2
H_2O modified	26.9	21.5	2.6	48.7	0.4
ACN control	27.3	17.7	0.3	54.5	0.2
ACN modified	20.2	34.4	3.4	38.1	4.0

The ratio of Mg and O for all samples is approximately 2 (Appendix Table A.1), indicative of the Mg:O ratio in $Mg(OH)_2$.

It is also clear that both modified samples have significantly greater amounts of nitrogen and carbon with respect to the other elements. Although present in the survey scans, peaks in the N 1s region narrow scans are only visible for samples modified with NBD

(Figure 11). The three peaks located at 400.0 eV, 402.8 eV, and 405.6 eV corresponds to a reduced N species ($-NH_2$ or $-N=N-$), a protonated imine ($R=N(H^+)-R$),[65] a protonated azo group ($R-N=N(H^+)-R$)[65–67] or diazonium ion ($-N_2^+$),[65,68] and $-NO_2$ functionality, respectively.[60] Reduction of $-NO_2$ may yield NH_2 while azo groups are included into the film as it grows (Scheme 1.1b). For the samples reacted with NBD, the reaction medium results in different ratios of nitro:amine/azo, with water the ratio is 1.1 and ACN it is 1.7. While there have been some reports that NO_2 groups can be reduced to NH_2 during XPS measurements,[60,69] this is less likely to occur with the laboratory-based XPS instrument used here than with synchrotron measurements. It is most reasonable to assume that the reduced N originates in azo linkages and it is clear that in water the film growth mechanism is more shifted towards azo than in ACN (Scheme 1.1b). A larger formation of azo linkages in H_2O agree with the assessment of 1 mM NBD solution resulting in a coloured film on Mg. Interestingly, reduction to the amine would allow for additional diazotisation and grafting of a bioactive layer, instead of in situ grafting of ABD which cannot be isolated as a salt.[70] The lack of any peak in the N 1s region in the unmodified samples indicates the presence of a nitro and azo functional groups on the surface.

The peak at 402.8 eV is interesting as it could represent a positively charged imine species or to a diazonium residual.[65–67] If it corresponds to the diazonium group, it shows that diazonium ions are trapped within the film or adsorbed to the surface. However, diazonium ions have two peaks of equal intensity around 403.8 eV and 405.1 eV,[71] which are not visible in either of the modified samples' spectra. Also, IR showed no peak corresponding to the diazonium ion, indicating that this XPS peak is probably the result of something else. If it is the imine species, it probably represents a protonated azo group (diazenium-like, Figure 12). It would be interesting to see how this forms and how it relates to the formation of multilayer films.[72] Further investigation into the formation of this peak is undoubtedly required.

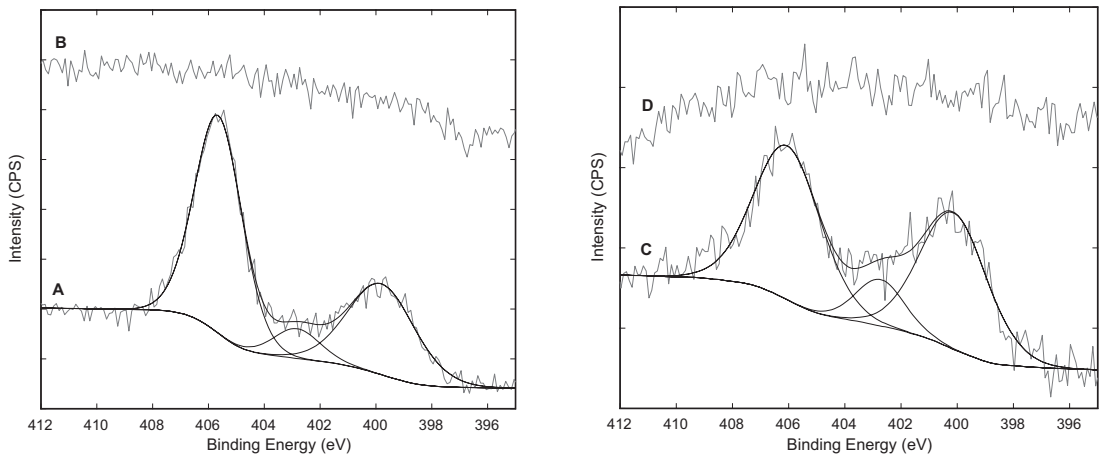

Figure 11. N 1s XPS spectra for (A) Mg reacted with 25 mM NBD in water; (B) ACN control; (C) Mg reacted with 25 mM NBD in water; (D) water control. Scale bar is equal to 50 CPS.

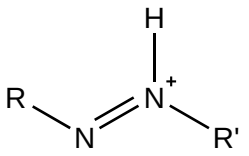

Figure 12. Diazenium ion

Figure 13 compares the narrow scan C 1s spectra of modified and unmodified samples within the same grafting medium. Four peaks can be found within this region at 284.8, 286.0, 289.2, 290.5 eV and correspond to aliphatic carbon (C−C, C−H), alcohols and ethers (C−O−H, C−O−C), carbonyl groups (COOH, −C(=O)−R), and carbonates (CO_3^{2-}). Adventitious carbon is present on all samples, but for both the sample reacted with NBD, the ratio and intensity of the aliphatic and C−O chemical environments increase compared to carbonyl and carbonate peaks increases.

Table 9 shows that after modification there is a greater amount of C−C and C−H, and C−O on the surface. More C−C may indicate the presence of the aromatic ring and the more C−O could results from the presence of C−N bonds which has a binding energy similar to C−O, however, it could also be caused if grafting occurs via a Mg−O−Ar linkage directly on the surface.

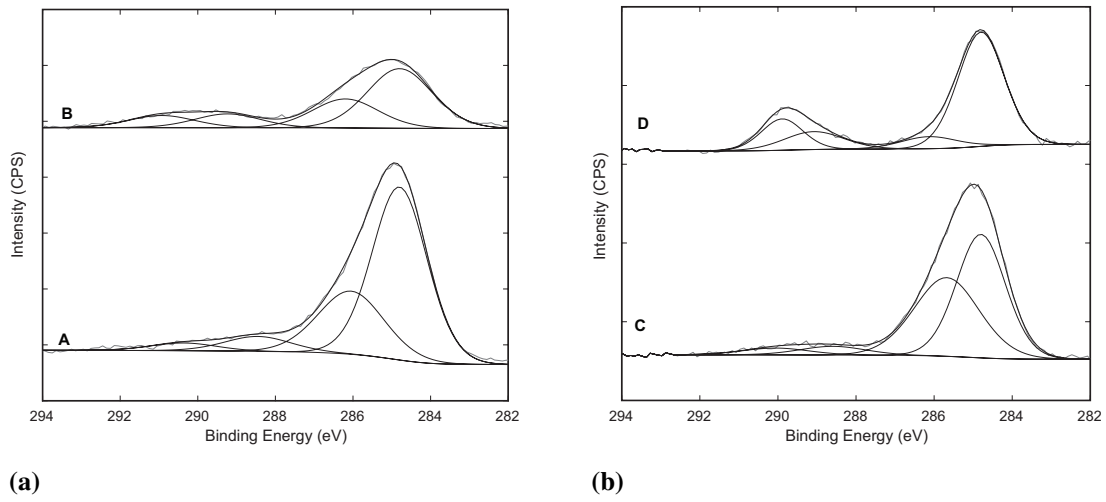

Figure 13. C 1s XPS spectra for (A) Mg reacted with 25 mM NBD in water; (B) ACN control; (C) Mg reacted with 25 mM NBD in water; (D) water control. Scale bar is equal to 500 CPS.

In the survey scan of the samples modified with NBD in water and ACN, there is a peak at 685 eV. This peak may correspond to MgF_2 which has this binding energy.[73] The binding energy of fluorine from the BF_4^- ion is 687 eV[74] which does not correlate to this peak. The decomposition of the BF_4^- ion would have to occur if F is on the surface and would explain the lack of a peak in the B 1s region at 195 eV.[75] A similar increase in the F 1s peak was observed by Berisha et al.[76] upon modification of Al in aqueous acid solution (0.01 M H_2SO_4) using $NBDBF_4$ (10 mM), they too were unsure how the phenomenon occurred. Further investigation into whether the BF_4^- ion interacts with Mg should be done to determine the cause of this peak, including higher resolution narrow

Table 9: Ratio of the peak area corresponding to aliphatic carbon (peak 1) to the remaining three C 1s peaks found on Mg. Peak 2 is C−O peak, Peak 3 is the carbonyl peak, and Peak 4 are carbonates. Samples are: H_2O control; Mg modified in water with 25 mM NBD; ACN control; Mg modified in ACN with 25 mM

Sample	Ratio to peak 1		
	Peak 2	Peak 3	Peak 4
H2O control	7.76	4.96	4.07
H2O modified	1.18	10.57	13.36
ACN control	2.03	4.24	4.84
ACN modified	2.28	9.65	18.73

scan measurements of the F 1s and B 1s regions.

In summary, XPS confirms the presence of nitro groups on the surface and the formation of multilayer films due to the presence of azo groups. The presence of NP films also indicates that sonication cannot remove this coating from the surface demonstrating that the coating is covalently coupled to the surface. The increase in C−O peak at 286 eV may reveal the grafting mechanism through the surface oxygen as opposed to with the metal.

3.2.4 Infrared Spectroscopy of EBD Modified Surfaces

To investigate the prospects of grafting thin ethynylphenyl (EP) films to Mg, a similar study to the NP grafted films above was conducted. Using Milli-Q water and ACN as the grafting media, it was expected that similar results to NBD would be observed.

The substrates modified in H_2O reacted almost immediately in solution, discolouring the surface within a minute and forming a thick film after 4 h. The sample modified using EBD with a concentration of 25 mM lost this layer due to sonication. Since these films have been described above (Section 3.2), they will not be discussed further.

The samples modified in ACN showed no visual change to the surface, indicating that if modification has occurred, the resulting layer must be very thin. To investigate this, IR spectra were collected (Figure 14).

Compared to the NP grafted film, the spectra for EP are not as well defined. Peaks associated with ring-breathing modes are not seen in the modified samples, but it does appear that the presence of diazonium, once again, reduces any corrosion. The broad peak at 1410 cm^{-1} of the ACN control sample indicates the presence of corrosion products and is smaller with the modified samples. The lack of features could indicate that EBD is only physisorbed to the Mg surface and is removed via sonication. Further investigation into the grafting of EBD is required as an EP film would be very useful for click chemistry to attach a second bioactive polymer layer.

3.2.5 Corrosion Testing of 4-Nitrophenyl Thin Films

To test whether the thin NP films grafted from H_2O and ACN provided corrosion protection, LSV polarisation curves were conducted.

It is clear in the Tafel plots of Figure 15 that there is no change in the corrosion

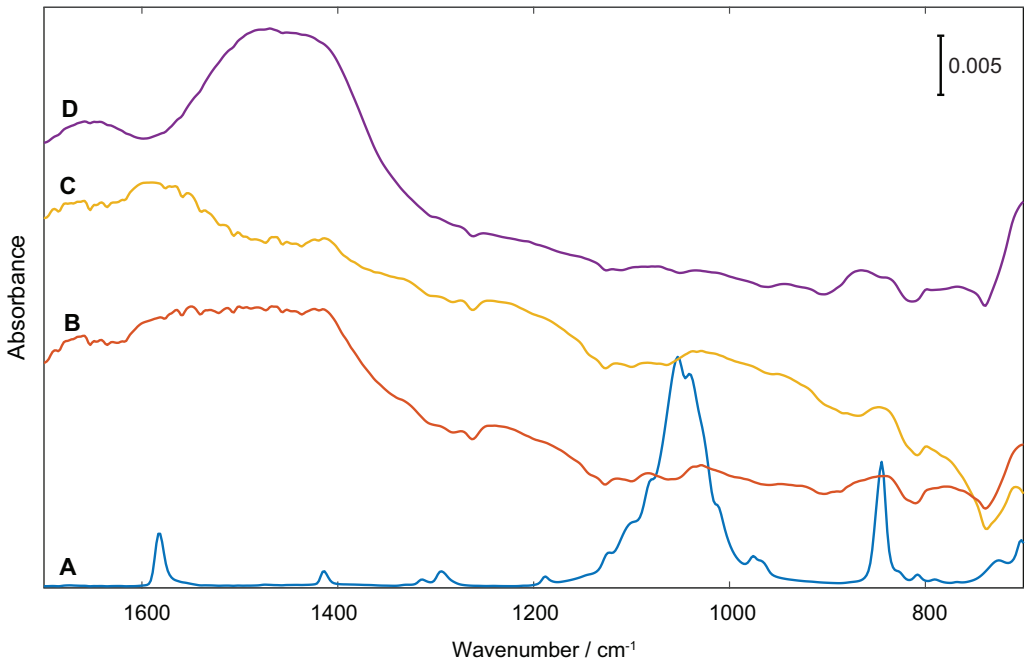

Figure 14. IR spectra of (A) $EBDBF_4$, scaled by 0.05; (B-C) Mg reacted in ACN with NBD with concentration: (B) 25 mM, (C) 10 mM; (D) ACN control. All samples modified for 4 h. Spectra were collected in ATR mode and are offset for clarity.

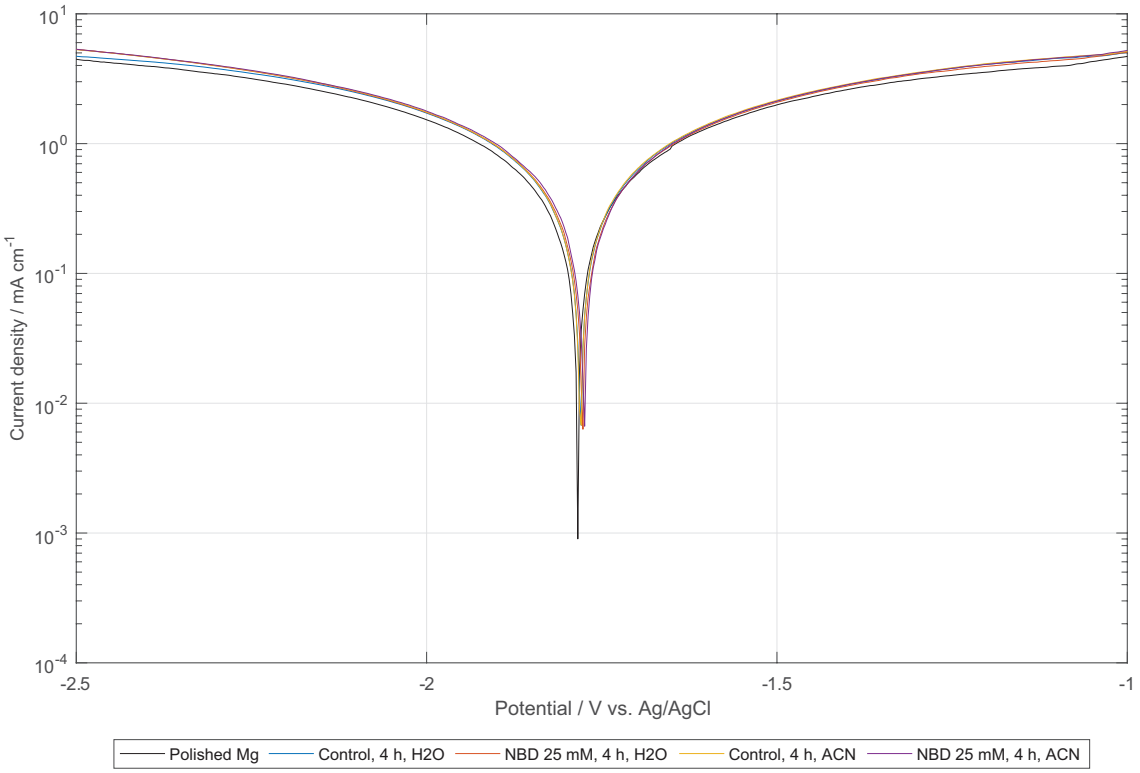

Figure 15. Tafel plot of polarisation curves of NP film on Mg substrate. LSV scanned at a rate of 1 mV s^{-1}.

properties of any of the substrates, indicating that the thin films provide no corrosion protection. Compared with the thicker films above (Section 3.1.2), this makes sense as only the thickest EP films provided corrosion protection. Considering these films are on the nano-scale, it is unlikely they can protect the surface without the addition a corrosion protection layer.

4 Conclusion

This study looked at the functionalisation of Mg using aryldiazonium chemistry to decrease the corrosion properties of the metal and successfully modified the surface with NP films.

NP and EP films were initially investigated using a buffered phosphate or carbonate aqueous solution as the grafting medium. It was found that the buffer solution caused corrosion on the Mg surface, resulting in the formation of a thick layer. This layer is probably caused by the precipitation of diazonium ions coupling in the bulk solution, with little reacting with the surface. Although films grafted from EBD showed substantial improvements to the corrosion properties, shifting E_{corr} positively by approximately 1.5 V and decreasing j_0 by six orders of magnitude, they would not be suitable for medical applications due to potentially carcinogenic properties and lack of biodegradability.

Preparation of nanoscale thick NP films was achieved in ACN and Milli-Q water. WCA, IR, and XPS confirm this. A decrease in the hydrophilicity of the surface was the initial indication that modification had occurred, and subsequent investigation using IR showed the characteristic symmetric and asymmetric NO_2 peaks on the surface. The lack of a peak within the $N_2{}^+$ vibrational region suggested that the aryl radical had formed and subsequently grafted to the surface. XPS confirmed this due to the presence of a nitro peak within the N 1s region. The simultaneous increase of the aliphatic carbon peak compared to carbon peaks associated with adventitious carbon also indicates the presence of the aromatic ring on the surface. Additionally, XPS may show that attachment of the NP layer occurs a surface oxygen, not through the Mg atom. The presence of fluorine on the surface requires further investigation with XPS.

Grafting of EBD in H_2O resulted in the formation of thick films, no matter the pH of solution tested. In ACN, IR results were inconclusive as to the presence of the film, and further work will be required as the ethynyl functionality is a very useful one for further on-surface chemistry. XPS analysis of EP films will provide additional information on the nature of the film. Importantly, the presence of an azo N would indicate the presence of a multilayer film.

Both water and ACN are suitable media for the reaction of NBD and Mg, but only ACN does not form a thick layer when using EBD. A concentration of 25 mM also appears to be optimal to obtain a suitable coating.

Coupling of a second layer which provides superior corrosion protection and simultaneously provides a bioactive surface to promote cell and bone adhesion is the next major step in this research. Depending on the functional group of the aryl layer, different

synthetic approaches will be required to prepare a suitable coating, such as cellulose or chitosan.

5 References

[1] Ponseti, I. V. History of Orthopaedic Surgery. *Iowa Orthop. J.* **1991**, *11*, 59–64.

[2] Staiger, M. P.; Pietak, A. M.; Huadmai, J.; Dias, G. Magnesium and Its Alloys as Orthopedic Biomaterials: A Review. *Biomaterials* **2006**, *27*, 1728–1734.

[3] Bessho, K.; Bessho, K.; Fujimura, K.; Fujimura, K. Experimental Long-Term Study of Titanium Ions Eluted from Pure Titanium Miniplates. *J. Biomed. Mater. Res.* **1995**, *29*, 901–904.

[4] Witte, F. The History of Biodegradable Magnesium Implants: A Review. *Acta Biomater.* **2010**, *6*, 1680–1692.

[5] Jacobs, J. J.; Gilbert, J. L.; Urban, R. M. Corrosion of Metal Orthopaedic Implants. *J. Bone Joint. Surg.* **1998**, *80*, 268–82.

[6] Zierold, A. A. Reaction of Bone to Various Metals. *Arch. Surg.* **1924**, *9*, 365–412.

[7] Huiskes, R.; Weinans, H.; Rietbergen, B. V. The Relationship between Stress Shielding and Bone Resorption around Total Hip Stems and the Effects of Flexible Materials. *Clin. Orthop. Relat. Res.* **1992**, *274*, 124–134.

[8] Mittal, R.; Morley, J.; Dinopoulos, H.; Drakoulakis, E. G.; Vermani, E.; Giannoudis, P. V. Use of Bio-Resorbable Implants for Stabilisation of Distal Radius Fractures: The United Kingdom Patients' Perspective. *Injury-Int. J. Care Inj.* **2005**, *36*, 333–338.

[9] Wolff, J. *The Law of Bone Remodelling*; Springer-Verlag: Berlin;Heidelberg;.

[10] Amini, A. R.; Wallace, J. S.; Nukavarapu, S. P. Short-Term and Long-Term Effects of Orthopedic Biodegradable Implants. *J. Long Term Effects Med. Implants* **2011**, *21*, 93–122.

[11] Bostman, O.; Pihlajamaki, H. Routine Implant Removal after Fracture Surgery: A Potentially Reducible Consumer of Hospital Resources in Trauma Units. *J. Trauma* **1996**, *41*, 846–849.

[12] Heise, S.; Virtanen, S.; Boccaccini, A. R. Tackling Mg Alloy Corrosion by Natural Polymer Coatings: A Review. *J. Biomed. Mater. Res. A* **2016**, *104*, 2628–2641.

[13] Zheng, Y. F.; Gu, X. N.; Witte, F. Biodegradable Metals. *Mater. Sci. Eng., R Rep.* **2014**, *77*, 1–34.

[14] Kulkarni, R. K.; Pani, K. C.; Neuman, C.; Leonard, F. Polylactic Acid for Surgical Implants. *Arch. Surg.* **1966**, *93*, 839–843.

[15] Middleton, J. C.; Tipton, A. J. Synthetic Biodegradable Polymers as Orthopedic Devices. *Biomaterials* **2000**, *21*, 2335–2346.

[16] Thamaraiselvi, T.; Rajeswari, S. Biological Evaluation of Bioceramic Materials - a Review. *Trends Biomater. Artif. Organs* **2004**, *18*, 9–17.

[17] Zheng, Y. F. *Magnesium Alloys as Degradable Biomaterials*; CRC Press, 2015.

[18] Friedrich, H. E.; Mordike, B. L. *Magnesium Technology: Metallurgy, Design Data, Applications*; Springer, 2006.

[19] Greenwood, N.; Earnshaw, A. *Chemistry of the Elements*; Pergamon Press, 1984.

[20] Burrows, A.; Holman, J.; Parsons, A.; Pilling, G.; Price, G. *Chemistry*^{3}*: Introducing Inorganic, Organic and Physical Chemistry*; Oxford University Press, 2013; p 1408.

[21] Nikolaychuk, P. A. The Third Dimension in Pourbaix Diagrams: A Further Extension. *J. Chem. Educ.* **2014**, *91*, 763–765.

[22] Lango, T.; Morland, T.; Brubakk, A. O. Diffusion Coefficients and Solubility Coefficients for Gases in Biological Fluids and Tissues: A Review. *Undersea Hyperb. Med.* **1996**, *23*, 247–272.

[23] Remennik, S.; Bartsch, I.; Willbold, E.; Witte, F.; Shechtman, D. New, Fast Corroding High Ductility Mg-Bi-Ca and Mg-Bi-Si Alloys, with No Clinically Observable Gas Formation in Bone Implants. *Mater. Sci. Eng., B* **2011**, *176*, 1653–1659.

[24] Witte, F.; Hort, N.; Vogt, C.; Cohen, S.; Kainer, K. U.; Willumeit, R.; Feyerabend, F. Degradable Biomaterials Based on Magnesium Corrosion. *Curr. Opin. Solid State Mater. Sci.* **2008**, *12*, 63–72.

[25] Witte, F.; Kaese, V.; Haferkamp, H.; Switzer, E.; Meyer-Lindenberg, A.; Wirth, C. J.; Windhagen, H. In Vivo Corrosion of Four Magnesium Alloys and the Associated Bone Response. *Biomaterials* **2005**, *26*, 3557–3563.

[26] Le, T.; Bhushan, V.; Sochat, M.; Chavda, Y. *First Aid for the Usmle Step 1 2017*, 27th ed.; McGraw-Hill Education / Medical, 2017.

[27] Wu, G. S.; Ibrahim, J. M.; Chu, P. K. Surface Design of Biodegradable Magnesium Alloys - a Review. *Surf. Coat. Technol.* **2013**, *233*, 2–12.

[28] Witte, F.; Fischer, J.; Nellesen, J.; Vogt, C.; Vogt, J.; Donath, T.; Beckmann, F. In Vivo Corrosion and Corrosion Protection of Magnesium Alloy LAE442. *Acta Biomater.* **2010**, *6*, 1792–1799.

[29] Gu, X. N.; Zheng, W.; Cheng, Y.; Zheng, Y. F. A Study on Alkaline Heat Treated Mg-Ca Alloy for the Control of the Biocorrosion Rate. *Acta Biomater.* **2009**, *5*, 2790–2799.

[30] Gu, X. N.; Li, N.; Zhou, W. R.; Zheng, Y. F.; Zhao, X.; Cai, Q. Z.; Ruan, L. Corrosion Resistance and Surface Biocompatibility of a Microarc Oxidation Coating on a Mg-Ca Alloy. *Acta Biomater.* **2011**, *7*, 1880–1889.

[31] Wang, Q.; Tan, L.; Xu, W.; Zhang, B.; Yang, K. Dynamic Behaviors of a Ca-P Coated AZ31B Magnesium Alloy During in Vitro and in Vivo Degradations. *Mater. Sci. Eng., B* **2011**, *176*, 1718–1726.

[32] Roy, A.; Singh, S. S.; Datta, M. K.; Lee, B.; Ohodnicki, J.; Kumta, P. N. Novel Sol-Gel Derived Calcium Phosphate Coatings on Mg4Y Alloy. *Mater. Sci. Eng., B* **2011**, *176*, 1679–1689.

[33] Singer, F.; Schlesak, M.; Mebert, C.; Hohn, S.; Virtanen, S. Corrosion Properties of Polydopamine Coatings Formed in One-Step Immersion Process on Magnesium. *ACS Appl. Mater. Interfaces* **2015**, *7*, 26758–26766.

[34] Zhang, J.; Dai, C. S.; Wei, J.; Wen, Z. H. Study on the Bonding Strength between Calcium Phosphate/Chitosan Composite Coatings and a Mg Alloy Substrate. *Appl. Surf. Sci.* **2012**, *261*, 276–286.

[35] Yliniemi, K.; Wilson, B. P.; Singer, F.; Hohn, S.; Kontturi, E.; Virtanen, S. Dissolution Control of Mg by Cellulose Acetate-Polyelectrolyte Membranes. *ACS Appl. Mater. Interfaces* **2014**, *6*, 22393–22399.

[36] Park, C. H.; Pant, H. R.; Kim, C. S. Effect on Corrosion Behavior of Collagen Film/Fiber Coated AZ31 Magnesium Alloy. *Dig. J. Nanomater. Bios.* **2013**, *8*, 1227–1234.

[37] Xu, X. H.; Lu, P.; Guo, M. Q.; Fang, M. Z. Cross-Linked Gelatin/Nanoparticles Composite Coating on Micro-Arc Oxidation Film for Corrosion and Drug Release. *Appl. Surf. Sci.* **2010**, *256*, 2367–2371.

[38] Lu, P.; Cao, L.; Liu, Y.; Xu, X.; Wu, X. Evaluation of Magnesium Ions Release, Biocorrosion, and Hemocompatibility of MAO/PLLA-Modified Magnesium Alloy WE42. *J. Biomed. Mater. Res., Part B* **2011**, *96B*, 101–109.

[39] Xu, L.; Yamamoto, A. In Vitro Degradation of Biodegradable Polymer-Coated Magnesium under Cell Culture Condition. *Appl. Surf. Sci.* **2012**, *258*, 6353–6358.

[40] Li, J. N.; Cao, P.; Zhang, X. N.; Zhang, S. X.; He, Y. H. In Vitro Degradation and Cell Attachment of a PLGA Coated Biodegradable Mg-6Zn Based Alloy. *J. Mater. Sci.* **2010**, *45*, 6038–6045.

[41] Pilling, N. B.; Bedworth, R. E. The Oxidation of Metals at High Temperatures. *J. Inst. Metals* **1923**, *29*, 529–582.

[42] Nordlien, J. H.; Ono, S.; Masuko, N.; Nisancioglu, K. A TEM Investigation of Naturally Formed Oxide Films on Pure Magnesium. *Corros. Sci.* **1997**, *39*, 1397–1414.

[43] Santamaria, M.; Di Quarto, F.; Zanna, S.; Marcus, P. Initial Surface Film on Magnesium Metal: A Characterization by X-Ray Photoelectron Spectroscopy (XPS) and Photocurrent Spectroscopy (PCS). *Electrochim. Acta* **2007**, *53*, 1314–1324.

[44] Yao, H. B.; Li, Y.; Wee, A. T. S. An XPS Investigation of the Oxidation/Corrosion of Melt-Spun Mg. *Appl. Surf. Sci.* **2000**, *158*, 112–119.

[45] Delamar, M.; Hitmi, R.; Pinson, J.; Saveant, J. M. Covalent Modification of Carbon Surfaces by Grafting of Functionalized Aryl Radicals Produced from Electrochemical Reduction of Diazonium Salts. *J. Am. Chem. Soc.* **1992**, *114*, 5883–5884.

[46] BeIanger, D.; Pinson, J. Electrografting: A Powerful Method for Surface Modification. *Chem. Soc. Rev.* **2011**, *40*, 3995.

[47] Pinson, J. Attachment of Organic Layers to Materials Surfaces by Reduction of Diazonium Salts. In *Aryl Diazonium Salts: New Coupling Agents in Polymer and Surface Science*; Chehimi, M. M., Ed.; Wiley-VCH: Weinheim, Germany, 2012.

[48] Podvorica, F. I.; Kanoufi, F.; Pinson, J.; Combellas, C. Spontaneous Grafting of Diazoates on Metals. *Electrochim. Acta* **2009**, *54*, 2164–2170.

[49] Bell, K. Surface Modification of Metal Oxide Materials with Aryldiazonium Ions. Ph.D Thesis, University of Canterbury, 2016.

[50] Mesnage, A.; Lefevre, X.; Jegou, P.; Deniau, G.; Palacin, S. Spontaneous Grafting of Diazonium Salts: Chemical Mechanism on Metallic Surfaces. *Langmuir* **2012**, *28*, 11776–11787.

[51] Schmidt, G.; Gallon, S.; Esnouf, S.; Bourgoin, J. P.; Chenevier, P. Mechanism of the Coupling of Diazonium to Single-Walled Carbon Nanotubes and Its Consequences. *Chemistry-a European Journal* **2009**, *15*, 2101–2110.

[52] Dunker, M. F. W.; Starkey, E. B.; Jenkins, G. L. The Preparation of Some Organic Mercurials from Diazonium Borofluorides. *J. Am. Chem. Soc.* **1936**, *58*, 2308–2309.

[53] Stalder, A. F.; Melchior, T.; Muller, M.; Sage, D.; Blu, T.; Unser, M. Low-Bond Axisymmetric Drop Shape Analysis for Surface Tension and Contact Angle Measurements of Sessile Drops. *Colloid Surf. A-Physicochem. Eng. Asp.* **2010**, *364*, 72–81.

[54] Melton, C.; Wilkes, R.; Staiger, M.; Downard, A. J. Novel Coatings for Improving the Corrosion Resistance of Magnesium Biomedical Implants. 2016; Unpublished Work.

[55] Seidell, A. *Solubilities of Inorganic and Metal Organic Compounds: A Compilation of Quantitative Solubility Data from the Periodical Literature*, 3rd ed.; D. van Nostrand Company: New York, 1940.

[56] Wen, Z.; Wu, C.; Dai, C.; Yang, F. Corrosion Behaviors of Mg and Its Alloys with Different Al Contents in a Modified Simulated Body Fluid. *J. Alloys Compd.* **2009**, *488*, 392–399.

[57] ECHA, Summary of Classification and Labelling - Phenylacetylene. 2017; https://echa.europa.eu/information-on-chemicals/cl-inventory-database/-/discli/details/103798.

[58] Kim, Y.; Go, S.; Ahn, Y. Fabrication of a Superhydrophobic Surface with Flower-Like Microstructures with a One-Step Immersion Process. *Bull. Korean Chem. Soc.* **2013**, *34*, 3495–3498.

[59] Tessier, L.; Deniau, G.; Charleux, B.; Palacin, S. Surface Electroinitiated Emulsion Polymerization (SEEP): A Mechanistic Approach. *Chem. Mater.* **2009**, *21*, 4261–4274.

[60] Hinrichs, K.; Katy, R.; Rappich, J.; Chehimi, M. M.; Pinson, J. Analytical Methods for the Characterization of Aryl Layers. In *Aryl Diazonium Salts: New Coupling Agents in Polymer and Surface Science*; Chehimi, M. M., Ed.; Wiley-VCH: Weinheim, Germany, 2012.

[61] Farquhar, A. K.; Dykstra, H. M.; Waterland, M. R.; Downard, A. J.; Brooksby, P. A. Spontaneous Modification of Free-Floating Few-Layer Graphene by Aryldiazonium Ions: Electrochemistry, Atomic Force Microscopy, and Infrared Spectroscopy from Grafted Films. *J. Phys. Chem. C* **2016**, *120*, 7543–7552.

[62] Pandurangappa, M.; Ramakrishnappa, T.; Compton, R. G. Functionalization of Glassy Carbon Spheres by Ball Milling of Aryl Diazonium Salts. *Carbon* **2009**, *47*, 2186–2193.

[63] Ricci, A.; Bonazzola, C.; Calvo, E. J. An FT-IRRAS Study of Nitrophenyl Mono- and Multilayers Electro-Deposited on Gold by Reduction of the Diazonium Salt. *PCCP* **2006**, *8*, 4297–4299.

[64] Richner, G.; van Bokhoven, J. A.; Neuhold, Y. M.; Makosch, M.; Hungerbuhler, K. In Situ Infrared Monitoring of the Solid/Liquid Catalyst Interface During the Three-Phase Hydrogenation of Nitrobenzene over Nanosized Au on TiO_2. *PCCP* **2011**, *13*, 12463–12471.

[65] Roodenko, K.; Gensch, M.; Rappich, J.; Hinrichs, K.; Esser, N.; Hunger, R. Time-Resolved Synchrotron XPS Monitoring of Irradiation-Induced Nitrobenzene Reduc-

tion for Chemical Lithography. *The Journal of Physical Chemistry B* **2007**, *111*, 7541–7549.

[66] Kumar, S. N.; Bouyssoux, G.; Gaillard, F. Electronic and Structural Characterization of Electrochemically Synthesized Conducting Polyaniline from XPS Studies. *Surf. Interface Anal.* **1990**, *15*, 531–536.

[67] Kohut-Svelko, N.; Reynaud, S.; Dedryvère, R.; Martinez, H.; Gonbeau, D.; François, J. Study of a Nanocomposite Based on a Conducting Polymer: Polyaniline. *Langmuir* **2005**, *21*, 1575–1583.

[68] Liu, Y.-C.; McCreery, R. L. Raman Spectroscopic Determination of the Structure and Orientation of Organic Monolayers Chemisorbed on Carbon Electrode Surfaces. *Anal. Chem.* **1997**, *69*, 2091–2097.

[69] Roodenko, K.; Gensch, M.; Rappich, J.; Hinrichs, K.; Esser, N.; Hunger, R. Time-Resolved Synchrotron XPS Monitoring of Irradiation-Induced Nitrobenzene Reduction for Chemical Lithography. *J. Phys. Chem. B* **2007**, *111*, 7541–7549.

[70] Mévellec, V.; Roussel, S.; Tessier, L.; Chancolon, J.; Mayne-L'Hermite, M.; Deniau, G.; Viel, P.; Palacin, S. Grafting Polymers on Surfaces: A New Powerful and Versatile Diazonium Salt-Based One-Step Process in Aqueous Media. *Chem. Mater.* **2007**, *19*, 6323–6330.

[71] Finn, P.; Jolly, W. L. Nitrogen 1s Binding-Energies of Some Azide, Dinitrogen, and Nitride Complexes of Transition-Metals. *Inorg. Chem.* **1972**, *11*, 1434.

[72] Doppelt, P.; Hallais, G.; Pinson, J.; Podvorica, F.; Verneyre, S. Surface Modification of Conducting Substrates. Existence of Azo Bonds in the Structure of Organic Layers Obtained from Diazonium Salts. *Chem. Mater.* **2007**, *19*, 4570–4575.

[73] Murch, G. E.; Thorn, R. J. Relation between Orbital Binding Energies and Ionicities in Alkali and Alkaline Earth Flourides. *J. Phys. Chem. Solids* **1980**, *41*, 785–791.

[74] Moulder, J.; Chastain, J. *Handbook of X-Ray Photoelectron Spectroscopy: A Reference Book of Standard Spectra for Identification and Interpretation of XPS Data*; Physical Electronics Division, Perkin-Elmer Corporation, 1992.

[75] Strohmeier, B. R. Surface Characterization of Aluminum Foil Annealed in the Presence of Ammonium Fluoborate. *Appl. Surf. Sci.* **1989**, *40*, 249–263.

[76] Berisha, A.; Hazimeh, H.; Galtayries, A.; Decorse, P.; Kanoufi, F.; Combellas, C.; Pinson, J.; Podvorica, F. I. Grafting of an Aluminium Surface with Organic Layers. *RSC Advances* **2016**, *6*, 78369–78377.

6 Appendix

6.1 Pilling-Bedworth ratio

$$R_{\mathrm{PB}} = \frac{V_{\mathrm{oxide}}}{V_{\mathrm{metal}}} = \frac{\mathrm{M}_{\mathrm{oxide}} \cdot \rho_{\mathrm{metal}}}{n \cdot \mathrm{M}_{\mathrm{metal}} \cdot \rho_{\mathrm{oxide}}} \tag{6.1}$$

- $R_{\mathrm{RB}} < 1$: the oxide coating layer is too thin, likely broken and provides no protective effect
- $1 < R_{\mathrm{RB}} < 2$: the oxide coating passivates and provides a protecting effect against further surface oxidation (e.g. Al)
- $R_{\mathrm{RB}} > 2$: the oxide coating chips off and provides no protective effect (e.g. Fe)

6.2 Balz-Schiemann reaction

The formation of aryl fluorides via the diazotisation of aryl amines and subsequent thermal or photochemical decomposition of the tetrafluoroborate salt.

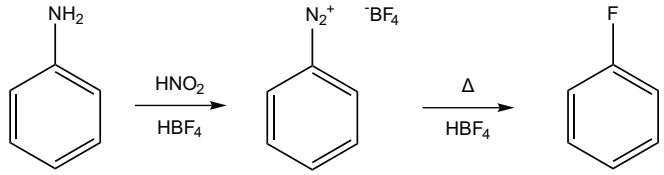

Scheme A.1. Balz-Schiemann reaction

6.3 Magnesium Substrate Photographs

(a) **(b)** **(c)** **(d)**

Figure A.1. Mg substrate after exposure to PB for certain time (Table 4).

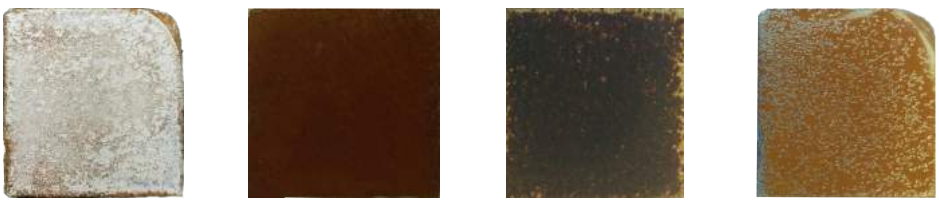

(a) **(b)** **(c)** **(d)**

Figure A.2. Mg substrate after exposure to PB and NBD under certain conditions as shown in Table 4.

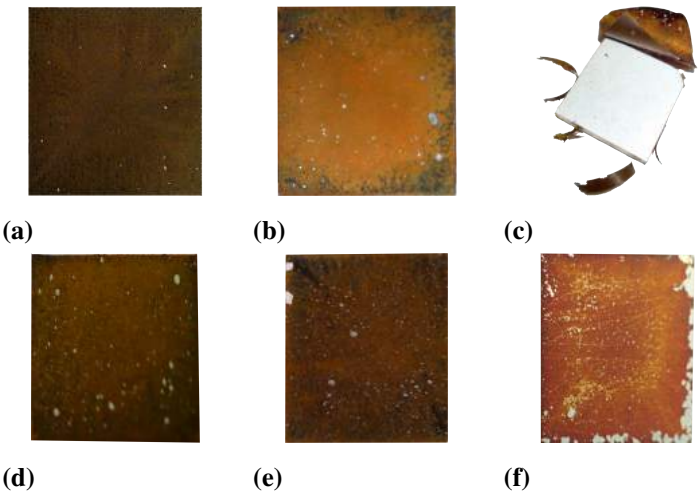

Figure A.3. Mg substrate after exposure to PB and EBD for certain time (Table 4).

Figure A.4. Photograph of surfaces of **(a)** H_2O control and **(b)** ACN control. Reacted for 4 h.

6.4 IR Spectra Assignments

(a) **(b)** **(c)**

Figure A.5. Photograph of Mg surface after reaction in: **(a)** 1 mM NBD; **(b)** 10 mM NBD; and **(c)** 25 mM NBD aqueous solutions. Reacted for 4 h. Conditions referred to in Table 5.

(a) 10 mM, H2O **(b)** **(c)** **(d)**

Figure A.6. Photograph of Mg surface after reaction in: **(a)** 10 mM EBD in water; **(b)** 25 mM EBD in water; **(c)** 10 mM EBD in ACN; **(d)** 25 mM EBD in ACN solutions. Reacted for 4 h. Conditions referred to in Table 5.

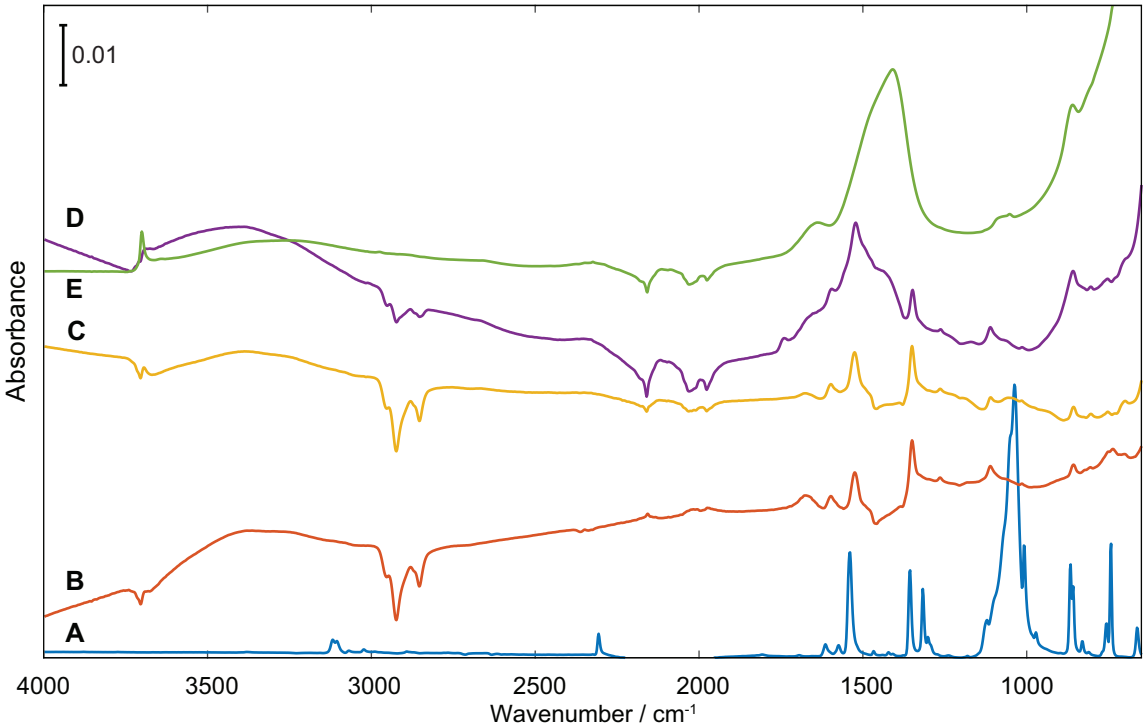

Figure A.7. R spectra of (A) $NBDBF_4$, scaled by 0.01; (B-D) Mg reacted in water with NBD with concentration: (B) 25 mM, (C) 10 mM, (D) 1 mM; (E) Mg reacted with 25 mM NBD ACN solution; (F) water control. All samples modified for 4 h. Spectra were collected in ATR mode and are offset for clarity.

6.5 XPS Spectra

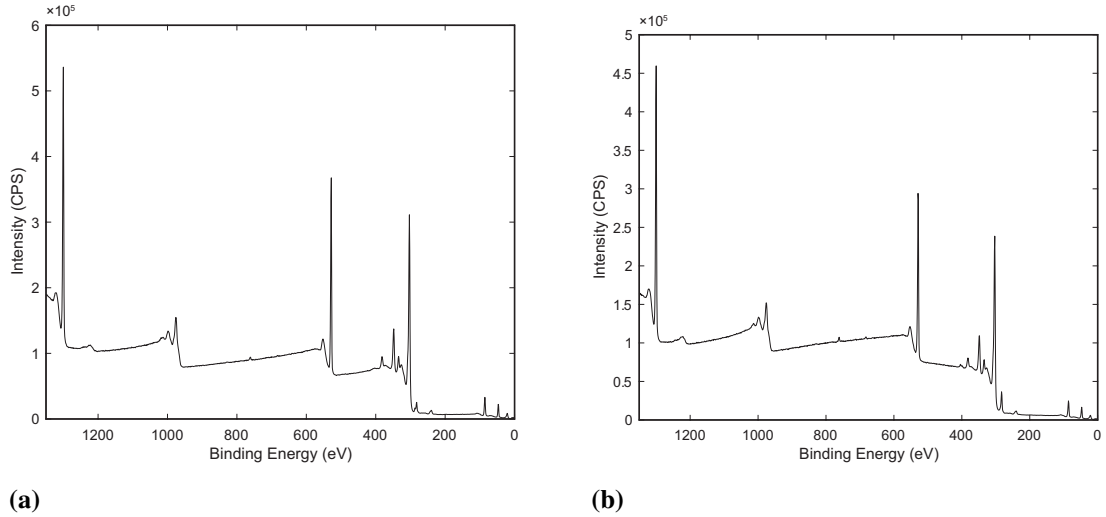

(a) **(b)**

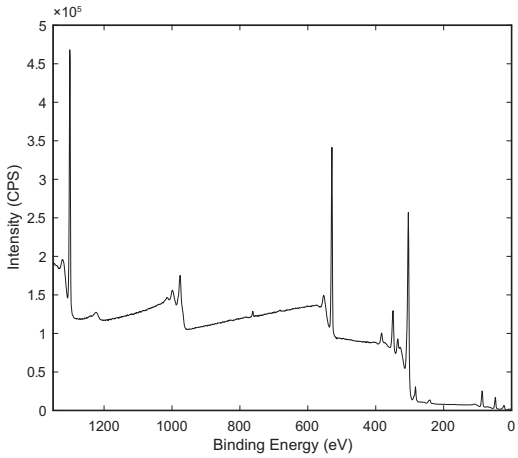

(c) XPS spectra of ACN control Mg.

Figure A.8. Survey spectra of remaining Mg samples from Figure 10. **(a)** H2O control Mg; **(b)** Mg reacted with 25 mM NBD in water; **(c)** ACN control. Reacted for 4 h.

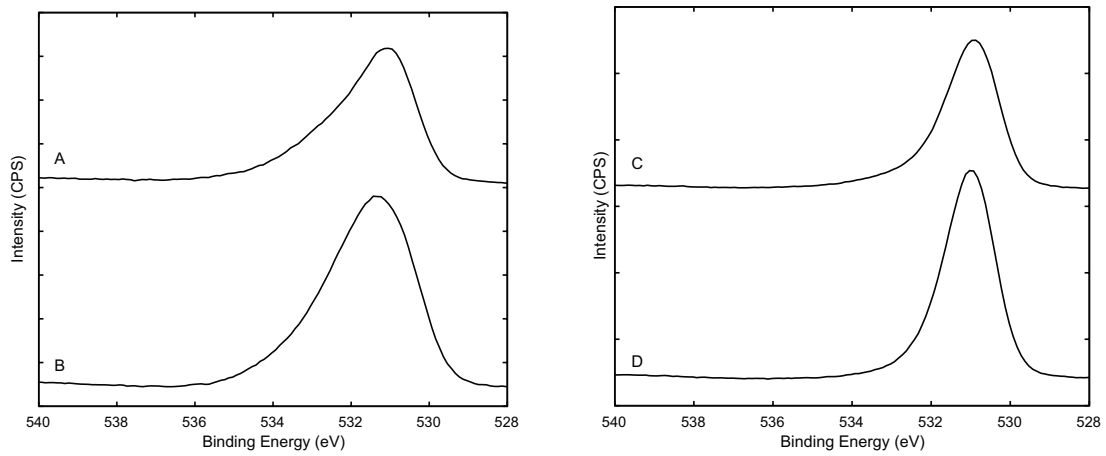

(a) **(b)**

Figure A.9. O 1s XPS spectra for: A) Mg reacted with 25 mM NBD in water; B) ACN control; C) Mg reacted with 25 mM NBD in water; D) water control. Scale bar is equal to **(a)** 2000 CPS and **(b)** 5000 CPS.

Table A.1: Ratio between elemental percentage from XPS data (Table 8). **(a)** with respect to Mg 1s; **(b)** with respect to C 1s; **(c)** with respect to N 1s; **(d)** with respect to O 1s. **X** is polished Mg; **A** is the H_2O control, **B** reacted with 25 mM NBD in water, **C** ACN control; **D** reacted with 25 mM NBD in ACN.

(a)

Mg 1s	**X**	**A**	**B**	**C**	**D**
Mg 1s	1.0	1.0	1.0	1.0	1.0
C 1s	1.4	0.5	0.8	0.6	1.7
N 1s	0.0	0.0	0.1	0.0	0.2
O 1s	2.7	1.9	1.8	2.0	1.9
F 1s	0.0	0.0	0.0	0.0	0.2

(b)

C 1s	**X**	**A**	**B**	**C**	**D**
Mg 1s	0.7	2.1	1.3	1.5	0.6
C 1s	1.0	1.0	1.0	1.0	1.0
N 1s	0.0	0.1	0.1	0.0	0.1
O 1s	2.0	4.0	2.3	3.1	1.1
F 1s	0.0	0.0	0.0	0.0	0.1

(c)

N 1s	**X**	**A**	**B**	**C**	**D**
Mg 1s	-	31.1	10.5	94.1	6.0
C 1s	-	15.0	8.4	61.1	10.2
N 1s	-	1.0	1.0	1.0	1.0
O 1s	-	59.1	19.1	187.8	11.3
F 1s	-	0.2	0.2	0.8	1.2

(d)

O 1s	**X**	**A**	**B**	**C**	**D**
Mg 1s	0.4	0.5	0.6	0.5	0.5
C 1s	0.5	0.3	0.4	0.3	0.9
N 1s	0.0	0.0	0.1	0.0	0.1
O 1s	1.0	1.0	1.0	1.0	1.0
F 1s	0.0	0.0	0.0	0.0	0.1